Evaluation of Arctic sea ice thickness simulated by AOMIP models

Mark Johnson[1], Andrey Proshutinsky[2], Yevgeny Aksenov[3], An T. Nguyen[4], Ron Lindsay[5], Christian Haas[6], Jinlun Zhang[5], Nikolay Diansky[7], Ron Kwok[8], Wieslaw Maslowski[9], Sirpa Hakkinen[10], Igor Ashik[11], Beverly de Cuevas[3].

[1]Institute of Marine Science, University of Alaska Fairbanks, Fairbanks, AK, USA

[2]Wood Hole Oceanographic Institution, Woods Hole, MA, US

[3]National Oceanography Centre, Southampton, Southampton, UK

[4]Massachusetts Institute of Technology, Cambridge, MA, USA

[5]Polar Science Center, University of Washington, Seattle, WA, USA

[6]University of Alberta, Edmonton, Canada

[7] Institute of Numerical Mathematics Russian Academy of Sciences, Moscow, Russia

[8]Jet Propulsion Laboratory, Pasadena, CA, USA

[9]Naval Postgraduate School, Monterey, CA, USA

[10]Goddard Space Flight Center, Greenbelt, MD, USA

[11]Arctic and Antarctic Research Institute, St. Petersburg, Russia

Abstract

We compare results from six AOMIP model simulations with estimates of sea ice thickness obtained from ICESat, moored and submarine-based upward looking sensors, airborne electromagnetic measurements and drill holes. Our goal is to find patterns of model performance to guide model improvement. The satellite data is pan-arctic from 2004–2008, ice-draft data is from moored instruments in Fram Strait, the Greenland Sea and the Beaufort Sea from 1992–2008 and from submarines from 1975-2000. The drill hole data are from the Laptev and East Siberian marginal seas from 1982–1986 and from coastal stations from 1998-2009. While there are important caveats when comparing modeled results with measurements from different platforms and time periods such as these, the models agree well with moored ULS data. In general, the AOMIP models underestimate the thickness of measured ice thicker than about 2 m and overestimate thickness of ice thinner than 2 m. The simulated results are poor over the fast ice and marginal seas of the Siberian shelves. Averaging over all observational data sets, the better correlations and smaller differences from observed thickness are from the ECCO2 and UW models.

1. Introduction

Dramatic decreases in Arctic sea ice are predicted by some climate models to the degree that multiyear ice may be lost during this century. Critical to the accuracy and reliability of high latitude climate forecasts and a better understanding of sea ice dynamics and thermodynamics is the proper simulation of sea ice and its responses to atmospheric forcing across a range of temporal and spatial scales. Assessment of model performance regarding sea ice would include, at least, comparisons with observations of the interrelated sea ice characteristics of motion, strain, deformation, concentration, age, and thickness. Evaluation of modeled sea ice behavior, however, is limited by incomplete observational data across the scales that characterize sea ice growth, melt, motion, and divergence.

With the beginning of the satellite record in the late 1970s, sea ice concentration became widely available as a product derived from passive microwave brightness temperatures [*Gloersen et al.*, 1992]. However, estimating sea ice thickness is not straightforward although procedures for estimating thickness as well as velocity from the satellite record have been developed [*Laxon et al.*, 2003; *Kwok et al.*, 2004]. Thickness is important to estimates of sea ice survival probability over the melt season [*Untersteiner*, 1961] and its distribution appears to be undergoing rapid changes [*Wadhams*, 1990*; Rothrock et al.*, 1999; *Wadhams and Davis*, 2000].

The focus of this paper is on the ability of six coupled Arctic Ocean Model Intercomparison Project (AOMIP) models to simulate sea ice thickness and to identify trends and differences among the AOMIP model ice thickness results by comparing them with the broad range of observed sea ice thickness data that is now available. The observational data include a) gridded ice thickness derived from the ICESat satellite for ten campaigns from fall and winter 2004 through 2008, b) ice thickness transect data from electromagnetic airborne measurements (2001-2009), c) ice draft from 24 moored instruments equipped with upward looking sonars (ULS) and ice profiling sonars (IPS) from 1992 through 2008 from the Beaufort Sea, Fram Strait and the Greenland Sea, d) ice draft from submarines equipped with upward-looking sonar (1975-2000), e) ice thickness in drill-holes through sea ice from 187 sites taken in spring from 1982 through 1986 across the Siberian marginal seas, and f) fast ice thickness from 51 Russian coastal stations (1998-2009). As described below, all ice-draft data were converted to ice thickness.

For this paper a range of thickness measurements is important to assess model performance. When and where ice is thin and/or in low concentration there is potential for high speed drift that may lead to dynamically driven increases in thickness via deformation while at the same time provide the potential for ice growth thermodynamically. Therefore, it is important to know whether specific models perform differently when simulating "thin" versus "thick" sea ice.

Because of differences among model forcing, processes, and parameterizations even within a coordinated modeling project such as AOMIP, our goal here is to identify the agreement between modeled sea ice and observations in order to provide a foundation for model improvement. However, the complexity of isolating specific model attributes from among the full suite of parameterizations, forcing, and boundary conditions is beyond the scope of this paper. In the end, the utility of comparisons such as those done here may be assessed by the rate of model improvement.

2. **Summary of previous work**

Bourke and Garrett [1987] first reported on the mean ice thickness distribution in the Arctic Ocean from data taken between 1960 and 1982. *Rothrock et al.* [1999] showed that that the mean ice draft in most of the central portion of the Arctic Ocean had declined from 3.1 m in 1958–1976 to 1.8 m in the 1990s (a 40% decrease). The submarine ice draft data in the data release area (DRA) were fit with multiple linear regression expressions of location, time and season by *Rothrock* et al. [2008] for the period 1975-2000. They found the annual mean ice draft declined from a peak of 3.42 m in 1980 to a minimum of 2.29 m in 2000. ICESat ice thickness estimates for 2003–2008 for the same area of the Arctic Ocean as represented by the regression equations match well with the earlier submarine records [*Kwok and Rothrock*, 2009] and show a continued decline to less than 1.0 m in the DRA in the fall of 2007. *Wadhams and Davis* [2000] also found a decline in the ice draft at the pole of 43% from 1976 to 1996. *Winsor* [2001], however, found no trend in six cruises between the pole and the Beaufort Sea from the 1990's.

Airborne EM surveys by *Haas et al.* [2009] showed a thinning of 20% in the region of the North Pole between 1991 and 2004, with a sharp drop to only 0.9 m in the summer of 2007 related to the replacement of old ice by first-year ice.

Direct comparison of model results to observed sea ice thickness has been limited because pan-Arctic sea ice thickness data were not widely available at useful resolutions. The lack of observational data was carefully circumvented by *Gerdes and Koberle* [2007] who compared results from several IPCC modeled outputs against sea ice thickness from a hindcast model (AWI1) positively evaluated against other AOMIP models. They concluded that differences among the IPCC models were likely due to the different effective wind stress forcing and the coupling methodologies with the ocean, a conclusion consistent with studies showing that atmospheric forcing fields essentially drive the results of sea ice simulations [*Walsh and Crane,* 1992; *Bitz et al.*, 2002; *Hunke and Holland*, 2007] more so than the details of the sea ice model itself [*Flato et al,.* 2004].

For sea ice concentration, satellite-derived values were compared with several AOMIP models to show that they reproduced winter-time observations reasonably well when ice concentration was near 100% but underestimated the September ice concentration minimum [*Johnson et al*., 2007]. The variability among model results exceeded the variability among four satellite-derived observational data sets suggesting the need to further constrain model performance or reduce sensitivity to prescribed forcing.

Assessment of model performance using sea ice drift and deformation derived from satellite data indicates little agreement between modeled patterns of sea-ice deformation fields and the linear features produced from the RADARSAT Geophysical Processor System (RGPS) at days to seasons and from kilometers to near basin scale [*Kwok, et al.*, 2008]. Compared to the RGPS products, specific model shortcomings included slow ice drift along coastal Alaska and Siberia, poor temporal rates of regional ice cover divergence, and low deformation-related ice volume production.

Assessment of the ice age-thickness relationship using model results shows that for northern hemisphere–wide averages the notion of thicker ice being older is reasonable at decadal scales, but for specific years and at scales less than hundreds of kilometers, ice age is not a good proxy for ice thickness [*Hunke and Bitz,* 2009]. At interannual time scales, the northern hemisphere averaged ice age is not well correlated with any of the three common ice descriptors: thickness, area or volume.

This paper is organized as follows. In the next section we present the six different AOMIP models followed by a review of the data sets against which they are compared. A section on the methods used to prepare the model and observational data follow. Comparison between models and data use a Taylor diagram modified to retain units of ice thickness residuals and model-data correlations, and also examines the linear regressions between the model and observed data. The paper concludes with a discussion of options for model improvement and a summary.

3. **Models**

The AOMIP project and its models were described previously in *Holland et al.* [2007] with considerable detail to be found on the AOMIP web site [http://www.whoi.edu/projects/AOMIP]. The six models used are from the Goddard Space Flight Center (GSFC), Jet Propulsion Laboratory (Estimating the Circulation and Climate of the Ocean, Phase II -- ECCO2), Institute of Numerical Mathematics Ocean Model (INMOM) Russian Academy of Science, the National Oceanography Centre Southampton (ORCA), the Naval Postgraduate School (NPS) Arctic

Modeling Effort (NAME), and the University of Washington (UW). Specific sea ice parameters for these models are shown in Table 1

3.1 **GSFC**

The GSFC model is based on the generalized Princeton Ocean Model (POM) which can accommodate sigma-coordinates (the original POM), but also z-levels and a mixture of sigma and z-levels, as the vertical coordinate [*Blumberg and Mellor*, 1987; *Mellor et al.* 2002]. The results presented here are from a version which uses only z-levels. The vertical mixing coefficients are determined from 2.5 layer turbulence closure (*Mellor and Yamada*, 1974) which requires computation of the kinetic energy and kinetic energy times mixing length as additional prognostic quantities. The ocean model is coupled to a two-layer dynamic- thermodynamic snow-ice model where the sea ice is described as a generalized viscous medium [*Mellor and Kantha*, 1989; *Hakkinen and Mellor*, 1992; *Hakkinen and Geiger*, 2000]. Ice-ocean momentum, heat and salt exchange is described by a flow over a rough surface based on the theory of *Yaglom and Kader* [1974]. The solar radiation can penetrate below the ocean surface to distribute short-wave solar heating.

The model domain covers the Arctic Ocean and the North Atlantic and extending to 15^0S, with a horizontal resolution of 0.35-0.45 degrees. Vertical resolution is 26 levels ranging from 6m to 500m layer depths. Transport at the open boundaries is defined by an inflow of 0.8 Sv through Bering Strait, which equals the amount that exits through the model's southern boundary at approximately 15^0S. The monthly T and S are restored at the open boundary buffer zones, but no other restoring is used in the GSFC model.

The specifications for AOMIP coordinated model run forcing are adopted except the following: P-E from *Rasmusson and Mo* [1996], and the Sellers formula as in *Parkinson and*

Washington [1979] for short wave radiation instead of AOMIP recommendations; the model uses NCEP wind stress instead of AOMIP recommended wind forcing. The GSFC model results are from a cold start at January 1948 using daily NCEP Reanalysis data.

3.2 **ECCO2**

The Arctic domain of ECCO2 uses a regional configuration of the Massachusetts Institute of Technology general circulation model (MITgcm, [*Marshall et al.*, 1997; *Losch et al.*, 2010, *Nguyen et al.*, 2011]. The domain has southern boundaries at ~ 55^{o}N in the Atlantic and Pacific sectors. The grid is locally orthogonal with horizontal grid spacing of approximately 18 km. There are 50 vertical levels ranging in thickness from 10 m near the surface to approximately 450 m at a maximum model depth of 6150 m. The model employs the rescaled vertical coordinate "z*" of *Adcroft and Campin* [2004] and the partial-cell formulation of *Adcroft et al.* [1997], which permits accurate representation of the bathymetry. Bathymetry is from the S2004 (*W. Smith*, unpublished) blend of the *Smith and Sandwell* [1997] and the General Bathymetric Charts of the Oceans (GEBCO) one arc-minute bathymetric grid. The non-linear equation of state of *Jackett and McDougall* [1995] is used. Vertical mixing follows *Large et al.* [1994]. A 7th-order monotonicity-preserving advection scheme [*Daru and Tenaud*, 2004] is employed and there is no explicit horizontal diffusivity. Horizontal viscosity follows *Leith* [1996] but is modified to sense the divergent flow [*Fox-Kemper and Menemenlis*, 2008].

The ocean model is coupled to the MITgcm sea ice model described in *Losch et al*. [2010]. Ice mechanics follow a viscous-plastic rheology and the ice momentum equations are solved numerically using the line-successive-over-relaxation (LSOR) solver of *Zhang and Hibler* [1997]. Ice thermodynamics are represented using a zero-heat-capacity formulation and seven thickness categories. Salt rejection during sea-ice formation is explicitly treated with a subgrid salt plume parameterization [*Nguyen et al.,* 2009]. The model includes prognostic variables for snow thickness and for sea ice salinity. Boundary conditions are monthly and taken from the global optimized ECCO2 solution [*Menemenlis et al.,* 2008]. Initial conditions are from the World Ocean Atlas 2005 [*Antonov et al.,* 2006*; Locarnini et al.,* 2006]. Atmospheric boundary conditions are from the Japanese 25-year Reanalysis Project (JRA25, [*Onogi et al.,* 2007]. The integration period is from 1992-2008. A comprehensive assessment of the solution used in this study can be found in *Nguyen et al.* [2011] where the model solution is parameter optimized from 1992 to 2004 using ice thickness data from submarine and mooring ULS, sea ice concentration and velocity, and ocean hydrography.

3.3 **INMOM**

The INMOM is a "terrain following" sigma-coordinate ocean model [*Moshonkin et al.*, 2011]. The global version of the INMOM with low spatial resolution is used as the oceanic component of the IPCC climate model INMOM [*Volodin et al.*, 2010] presented in the IPCC Fourth Assessment Report [2007]. The present version of the model covers the North Atlantic (open boundary at approximately 20°S), Arctic Ocean, and Bering Sea regions including Mediterranean and Black Seas. A rotation of the model grid avoids the problem of converging meridians over the Arctic Ocean. The model North Pole is located at the geographical equator, 120°W. The 1/4° horizontal eddy-permitting resolution is used. There are 27 unevenly spaced vertical sigma-levels. A Laplacian operator along the geopotential surface is used for the lateral diffusion on the tracers and a bilaplacian operator along sigma-surface is used for the lateral viscosity on momentum. The vertical viscosity and diffusion coefficients are calculated by Monin-Obuhov-Kochergin [*Kochergin*, 1987] parameterization. The elastic-viscous-plastic (EVP) dynamic - thermodynamic sea ice model [*Hunke*, 2001; *Yakovlev*, 2009] is coupled to the ocean model. Surface forcing is from the CORE forcing dataset [*Large and Yeager,* 2004]. The surface turbulent fluxes are calculated using the bulk formulae. A climatological monthly runoff from CORE is applied along the coasts. Surface salinity is restored towards monthly climatology with a relaxation scale of approximately 12 days both for the open ocean and under sea-ice. Temperature and salinity restoring towards monthly climatology is used at the open boundaries.

3.4 **ORCA**

The ORCA model is a global z-level OGCM based on the NEMO ocean code [*Madec,* 2006] and uses the global tri-polar ORCA grid at ¼° horizontal resolution. The effective resolution is ~27.75 km at the equator increasing to 6-12 km in zonal and ~3 km in meridional directions in the Arctic Ocean, thus the model resolves large eddies in the Arctic Ocean and "permits" smaller ones. The configuration was developed by the DRAKKAR project and is described by *Barnier et al.* [2006] as the ORCA025-G70 configuration. The version of the model used here has a higher vertical resolution (64 vertical levels) than the ORCA025-G70, with thicknesses of the model levels ranging from ~6 m near the surface to ~204 m at 6000 m. The 'partial step' topography [*Adcroft et al.,* 1997, *Pacanowski & Gnanadesikan*, 1998] is used, whereby the bottom cell is variable and more able to represent small topographic slopes near the Arctic shelves, resulting in the more realistic along-shelf flow [e.g.*, Barnier et al,*. 2006; *Penduff et al*., 2007]. The ocean model is coupled asynchronously to the sea ice model every five oceanic time steps through a non-linear quadratic drag law [*Timmermann et al*., 2005].

The sea-ice model LIM2 [*Fichefet et al.,* 1997] is based on the Viscous-Plastic (VP) rheology with an elliptic yield curve [*Hibler*, 1979] and Semtner's 2-layer ice, 1-layer snow thermodynamics [*Semtner,* 1976]. The latter is updated with sea ice thickness distribution [*Fichefet et al.*, 1997]. Other features of the model are the positive-definite, second order, second moments conserving advection scheme [*Prather*, 1986], ice-thickness dependent *albedo* [*Payne*, 1972), lateral ice thermodynamics and a simple snow-ice formation mechanism due to hydrostatic imbalance [*Fichefet et al*., 1997]. Sea ice salinity is taken equal to 4, the average value of sea ice salinity in the Central Arctic Ocean. Heat exchange between the ocean and sea ice is calculated as a product from the departure of surface temperature from the salinity-dependent freezing point and friction velocity at the ice-ocean interface. Solar radiation penetrates snowless ice, increasing latent heat storage in brine pockets [*Fichefet et al.*, 1997].

Surface forcing is provided by the DRAKKAR Forcing Set 3 [*Brodeau et al.*, 2001]. This dataset is a combination of precipitation and downward longwave and shortwave radiation fields from the CORE forcing dataset [*Large and Yeager*, 2004] and 10-m wind, 2-m air temperature and 2-m specific humidity from the ECMWF ERA40 re-analysis product. The turbulent air/sea and air/ice fluxes are calculated by the model using the bulk formulae [*Large and Yeager*, 2004]. A climatological monthly runoff [*Dai and Trenberth*, 2002] is applied along the coasts. Surface salinity is restored towards monthly climatology with a relaxation scale of 180 days for the open ocean and 12 days under sea-ice.

3.5 **Naval Postgraduate School (NPS) Arctic Modeling Effort (NAME)**

The NPS pan-Arctic coupled ice-ocean model used in this study consists of a Hibler-type sea ice model (*Zhang and Hibler*, 1997) coupled to a regional adaptation of the Parallel Ocean Program (POP) [*Smith et al.*, 1992; *Smith and Gent*, 2002]. The sea ice model employs a viscous-plastic rheology, two ice thickness categories (mean ice thickness and open water), the zero-layer approximation of heat conduction through ice and a simplified surface energy budget (*Zhang et al.*, 1999; *Maslowski et al.*, 2000). The ice strength is parameterized in this model as a function of the mean grid-cell ice thickness, which tends to underestimate ice drift and deformation [*Maslowski and Lipscomb*, 2003; *Kwok et al.*, 2008]. The ocean model is a z-coordinate ocean model with an implicit free surface and 45 vertical levels, with layer thickness ranging from 5 m near the surface to 300 m at depth.

The model domain includes all sea-ice covered oceans and marginal seas of the northern hemisphere. It includes the Arctic Ocean, sub-Arctic seas and extends to ~30^0N in the North Pacific and to ~45^0N in the North Atlantic. Both components of the coupled model use identical horizontal grid configured at $1/12^0$ (~9 km) in a rotated spherical coordinate system to eliminate the North Pole singularity. The model lateral boundaries are solid and no mass flux is allowed through them however a virtual annual cycle salt flux is prescribed for most major rivers as a function of river run-off. Surface layer (0-5 m) temperature and salinity are restored toward monthly climatology [PHC; *Steele et al.*, 2001]) on timescales of 365 and 120 days, respectively.

The model was forced with daily-average atmospheric fields (downward longwave and shortwave radiation, surface air temperature, specific humidity, wind velocity and stress) from the European Centre for Medium-range Weather Forecasts (ECMWF) 1979–1993 reanalysis and 1994-2004 operational products. Additional details of model configuration, initialization and integrations can be found in *Maslowski et al.* [2004, 2008].

3.6 **University of Washington (UW)**

The UW model is the coupled pan-arctic ice–ocean modeling and assimilation system (PIOMAS), a regional version of the global Parallel Ocean and Ice Model (POIM) [*Zhang and Rothrock*, 2003]. The sea ice model is the multi-category thickness and enthalpy distribution (TED) sea ice model [*Zhang and Rothrock*, 2001; *Hibler*, 1980]. It employs a teardrop plastic rheology [*Zhang and Rothrock*, 2005], a mechanical redistribution function for ice ridging [*Thorndike et al*., 1975; *Hibler*, 1980], and a LSR (line successive relaxation) dynamics model to solve the ice momentum equation [*Zhang and Hibler*, 1997]. The TED ice model also includes a snow thickness distribution model following *Flato and Hibler* [1995]. The ocean model is based on the Parallel Ocean Program (POP) developed at Los Alamos National Laboratory [*Smith et al.*, 1992]. The model domain of PIOMAS covers the northern hemisphere north of 48ºN. The POP ocean model has been modified to incorporate open boundary conditions [*Zhang and Steele*, 2007] so that PIOMAS is able to be one-way nested to a global POIM [*Zhang*, 2005] with open boundary conditions along 49ºN. The PIOMAS finite-difference grid is based on a generalized orthogonal curvilinear coordinate system with the "north pole" of the model grid placed in Greenland. The model horizontal resolution ranges from 6 to 75 km with a mean resolution of 22 km for the Arctic, Barents, and GIN (Greenland-Iceland-Norwegian) seas, and Baffin Bay. The TED sea ice model has 12 categories each for ice thickness, ice enthalpy, and snow depth. The centers of the 12 ice thickness categories are 0, 0.26, 0.71, 1.46, 2.61, 4.23, 6.39, 9.10, 12.39, 16.24, 20.62, and 25.49 m. The POP ocean model has 30 vertical levels of varying thicknesses to resolve surface layers and bottom topography. The first 13 levels are in the upper 100 m and the upper six levels are each 5 m thick. The model bathymetry is obtained by merging the IBCAO (International Bathymetric Chart of the Arctic Ocean) dataset and the ETOPO5 (Earth Topography Five Minute Gridded Elevation Data Set) dataset [see *Holland*, 2000]. PIOMAS is forced by daily NCEP/NCAR reanalysis [*Kalnay et al*., 1996] surface forcing fields, i.e., 10 m surface winds, 2 m surface air temperature (SAT), specific humidity, precipitation, evaporation, downwelling longwave radiation, sea level pressure, and cloud fraction. Cloud fraction and SAT are used to calculate downwelling shortwave radiation following *Parkinson and Washington* [1979]. Model forcing also includes river runoff of freshwater in the Arctic Ocean. Climatological river runoff (i.e., no interannual variability) is provided as in the work of *Hibler* *and Bryan* [1987]. The calculations of surface momentum and radiation fluxes follow *Zhang and Rothrock* [2003] and differ from the specifications for the AOMIP coordinated runs. No climate restoring is allowed. No data assimilation is performed for this study, although PIOMAS is able to assimilate ice concentration and sea surface temperature data.

4. Observational data

Ice thickness from models is compared with observed thickness, ice draft or freeboard that has been converted to thickness. Conversion for undeformed ice without snow or melt ponds is straightforward. Assuming ice is in hydrostatic equilibrium with seawater, ice thickness is the draft times the ratio of seawater density to sea-ice density. Snow cover, melt ponds and deformed ice provide sources of error. Still, it is not uncommon to use thickness as the product of draft and some constant. We use 1.115 [*Bourke and Paquette*, 1989] to convert draft to thickness.

Much of the data used in this study is available from the new Unified Sea Ice Thickness Climate Data Record [*Lindsay*, 2010]. This archive has summary statistics for moorings, submarines, aircraft, and satellite measurements of ice draft and ice thickness. The summary statistics include mean, minimum, maximum, and standard deviation of the measurement as well as the full probability density distribution. There are currently over 3000 samples in the archive which can be accessed along with documentation and metadata at http://psc.apl.washington.edu/sea_ice_cdr.

4.1 ICESat campaigns

Gridded Arctic Ocean sea ice thickness fields with resolution of 25 km × 25 km (Figure 1a) from 2004 through 2008 have been created from five fall and five winter ICESat campaigns [*Kwok et al.*, 2009]. There is typically a three to four month separation between the fall and winter campaigns. The duration, start and end dates of the fall and winter campaigns, shown in

Table 2, are variable. The five fall campaigns start between September 24th and October 25th and end between November 8th and November 27th. Winter campaigns start between February 17th and March 12th and end between March 21 and April 14th. We expect these shifts in the individual satellite campaign timing to introduce seasonal and interannual variability within the dataset, although it may not be particularly large as thicknesses represent near maximum end-of-winter and minimum end-of-summer data.

The ICESat thickness data are derived from freeboard (distance above the water line to top of the snow cover) obtained from the Geoscience Laser Altimeter System (GLAS). The methodology for determining freeboard, snow depth, and ice thickness from the 70 m footprint for ICESat is given by *Kwok et al*. [2007] and *Kwok et al*. [2009]. The empirical relationship between thickness and freeboard for the first year (FY) ice in late winter is discussed in *Alexandrov et al.* [2010].

Satellite grid point values were computed and a 50-km Gaussian smoothing applied. The satellite hole is filled using an interpolation procedure described in *Kwok et al*. [2009]. ICESat estimates [*Kwok et al*., 2009] of ice drafts are consistently within 0.5 m (one standard deviation) of profiles from a submarine cruise in mid-November of 2005, and four years of ice draft from moorings (BGEP-WHOI and AIM-IOS) in the Chukchi and Beaufort Seas. The gridded ICESat ice thickness estimates are available at the Jet Propulsion Laboratory at http://rkwok.jpl.nasa.gov/icesat/index.html. The error variance of the ICESat thickness data is (0.37 m^2) [*Kwok and Rothrock*, 2009]. The ICESat measurements, when converted to drafts, are smaller on average by 0.1±0.42 m than adjusted ULS submarine drafts (see Section 4.4) and by 0.14±0.51 m than ULS moored drafts [*Kwok et al*, 2009].

4.2 **Electromagnetic airborne soundings**

Thickness data were obtained using electromagnetic (EM) induction sounding that computes the distance to the ice/water-interface by evaluating the amplitude and phase of a secondary EM field induced by eddy currents in the seawater. With airborne measurements, the height of the EM instrument above the air-snow surface is measured with a laser altimeter. Ice thickness is then obtained from the difference of the EM distance measurement to the ice/water-interface and the laser height of the snow [*Haas et al.*, 2009], hence ice thickness from the EM measurements includes snow thickness.

The accuracy of the EM method is ±0.1 m over level ice under typical summer conditions [*Haas et al.*, 1997; *Pfaffling et al.*, 2007] with only small effects from melt ponds [*Haas et al.*, 1997; *Eicken et al.*, 2001]. The horizontal extent of induced eddy currents results in a measurement footprint area of up to 3.7 times the instrument height above the water [*Reid et al.*, 2006]. The measured, unconsolidated ridge thickness can be less than 50% of its "true" thickness [e.g., *Haas and Jochmann*, 2003], although the magnitude of this underestimate is uncertain. The EM thickness distributions are most accurate with respect to modal thickness, while mean thickness can still be used for relative comparisons between regions and years. Surveys were performed with helicopters and fixed-wing aircraft using a towed sensor ("EM-Bird") from icebreakers and land bases in various regions of the eastern and western Arctic [*Haas et al.*, 2006; *Haas et al.*, 2008; *Haas et al.*, 2009; *Haas et al.*, 2010]. Surveys have generally been performed in the April/May and August/September periods and data locations used in this paper are shown in Figure 2.

4.3 **Upward looking sonar and ice profiling sensors from moorings**

Eleven moorings with upward looking sonars (ULS) deployed in Fram Strait and the Greenland Sea (Figure 1b) by the Alfred Wegener Institute for Polar and Marine Research, Bremerhaven, Germany acquired almost 25 station-years of data between 2002 and 2004 as a contribution to the World Climate Research Programme's Arctic Climate System Study/Climate and Cryosphere (ACSYS/CliC) Project. The ice draft data are available from the Unified Sea Ice Thickness Climate Data Record as well as the National Snow and Ice Data Center web site with data descriptions *Witte and Fahrbach* [2005].

Sea ice draft data are available on the continental shelf of the Eastern Beaufort Sea for the period April 1990 through September 2003 from Ice Profiling Sonar (IPS) instruments deployed by H. Melling at the Institute for Ocean Sciences (IOS), Canada. Data are described in *Melling and Riedel* [2008] and references therein. Sea ice draft data in the central Beaufort Sea for the period 2003-2008 were acquired through the Beaufort Gyre Exploration Project (BGEP, A. Proshutinsky, PI). The point data are available at the Woods Hole Oceanographic Institute web site (http://www.whoi.edu/beaufortgyre/data.html).

Melling and Riedel [2004] estimate for their data an accuracy of ± 0.05 m draft for level ice. Draft will be overestimated on average in rough ice. The ACSYS/CliC Workshop [*Steffen*, 2004] on sea-ice thickness requires an accuracy of ± 0.05 m for draft for ULS and IPS and we use that figure here for all ULS data. We acknowledge that NSIDC has been alerted to an error in the way the bias correction was applied for the AWI data, but pending further clarification these data are used assuming the above accuracy.

4.4 **Upward Looking Sonar measurements from submarines**

Submarines have traversed the Arctic regularly since 1958 measuring the draft of the overhead sea ice using upward looking sonar (ULS). The processed and publicly available data (archived at NSIDC and available as 50-km averages at the Unified Sea Ice Thickness Climate Data Record) include 42 cruises from 1975 to 2000 covering 120,000 km of data. The cruises took place between April and November, although most of the data were collected in late spring (April-May) and in late summer-fall (August-October) [*Rothrock and Wensnahan*, 2007].

The draft data are produced for periods when the submarine was traveling in a straight line at constant speed and depth. The basic data product is ice draft along the cruise track (Figure 2). The data typically have a spacing of 1-8 m with a footprint size of 2-7 m depending on the submarine depth. Data segments vary in length from a few to several hundred kilometers.

Rothrock and Wensnahan [2007] identify the following submarine ice draft measurement errors: precision error; error in identifying open water (ice of zero draft); sound speed error; error caused by sonar footprint size variations; error from uncontrolled gain and thresholds; error due to vessel trim. There are also differences between analog versus digitally recorded data with paper charts biased toward thicker ice by over 0.30 m due to their coarser temporal resolution. The drafts are obtained from the "first return" or from the depth of the deepest ice within the footprint. They estimated the overall bias due to this effect of the submarine ULS data from the actual draft as +0.29 m with a standard deviation of ±0.25 m. A recent paper [*Rodrigues*, 2010] finds a bias based on the sonar beam width and ice roughness larger than that found by *Rothrock and Wensnahan* [2007]. For this study we have corrected for the submarine draft bias of +0.29 m described in *Rothrock and Wensnahan* [2007].

4.5 **Pack-ice and fast-ice measurements from drill holes**

Historical ice thickness data are available from the “Atlas of ice and snow of the Arctic Basin and Siberian Shelf Seas” [*Romanov*, 1995]. This data set contains sea ice and snow Spring (mid March – mid May) measurements collected during aircraft landings associated with the Soviet Union's historical *Sever* airborne and North Pole drifting station programs. The High-Latitude Airborne Annual Expeditions *Sever* took place in 1937, 1941, 1948-1952, and 1954-1993

[*Konstantinov and Grachev*, 2000]. The data set is derived from as few as 7 landings (1937) to nearly pan-arctic coverage in the 1970s. The data set contains measurements of 23 parameters, including a) ice thickness and snow depth on the runway and surrounding area, b) ridge, hummock, and sastrugi dimensions and areal coverage and c) snow density. The data used in this paper are a subset of those used to create the atlas “Morphometric Characteristics of Ice and Snow in the Arctic Basin” (self-published by Ilya P. Romanov in 1993 and republished by Backbone Publishing Company in 1995). Romanov provided these data to NSIDC in 1994 (see http://nsidc.org/data/g02140.html for full description and data in ASCII format). In this paper we use ice thickness data in the Spring from 1982 through 1986 (Figure 1b). The data were obtained at sites adjacent to the aircraft landing areas (undisturbed ice).

We also use data from 51 coastal stations where sea ice thickness was measured monthly through drill holes. The data represent thicknesses of the fast sea ice in the vicinity of the coastal station, mostly first-year ice, undeformed by ridging or rafting. Monthly data are available for 1998-2009. The data were provided by the Arctic and Antarctic Research Institute, St. Petersburg, Russia. Although these data and the data from the Romanov Atlas are unique, and the accuracy of such direct measurements is likely less than 0.05 m, we cannot make a formal statement regarding position error and accuracy.

5. **Methods**

All ice-draft data were converted to thickness as described above. In the following discussion, model minus observed thickness values are referred to as residuals, and thus the residuals are positive when the model overestimates the observed thickness. The observed data were monthly averaged except for the ICESat data which are provided as ~2-month averages. Where model results temporally overlapped the observed data, model ice thickness was extracted from the nearest model grid point and averaged into monthly means. We recognize that the observational data have very different spatial resolutions; moored instruments and drill holes produce point data, while the ICESat data were processed using a 50-km Gaussian smoothing, and the Unified Sea Ice Thickness Climate Data Record provides the statistical mean ice thickness at 50 km intervals for the submarine ULS data. We chose to compare the observed data with the nearest model grid point, an approach perhaps advantageous to models with finer resolution. For models with coarse resolution, a 50-km weighted average, which is used by *Rothrock and Wensnahan* [2007] might be advantageous. In this paper, we used the nearest model grid point to the observed data, formed monthly averages of model and observational data (~2 months for ICESat), and then computed residuals and correlations. This approach leads to consistent results, described below, across data sets and models.

Record-length correlation coefficients and residuals were computed from the monthly time series for each of the moored ULS and the 51 coastal stations data. Annual correlation coefficients and residuals were computed for the each of the ICESat, airborne EM, Romanov Atlas, and submarine data sets by averaging all data in the given year. Grand mean correlation coefficients and residuals for each observational platform were computed by averaging all 25 ULS time series and from all 51 Coastal Station time series, and averaging all years for the ICESat, airborne EM, Romanov Atlas, and submarine data. These differences should be kept in mind in the following discussion.

To show the correlation coefficients and residuals, a modified Taylor Diagram [*Taylor*, 2001] is used. In this diagram, the radial distance from the origin is the correlation coefficient (r=1 falls on the unit circle) and the rotation angle (θ) is proportional to residuals with $\pm\pi$ corresponding to residuals of ± 2 m (Figure 3).

A quantitative evaluation arises from the modified Taylor diagram where model performance is proportional to the area swept by the radial "tip" $(1-r)$ rotated from zero to the residual (θ). The result, $|(1-r)\theta|$ is used to rank the model performance.

Linear regressions are used to obtain relationships between the observed and modeled time series means and monthly means from the spatial data. We used annually averaged thickness for ICESat and Romanov Atlas, monthly averages using the multiple locations for the airborne EM and submarine ULS data, record-length means from the time series from moored ULS and the 51 Coastal Stations. Our purpose is to identify systematic biases in the simulations as a function of observed thickness. Statistical differences among the correlations and residuals are not discussed considering the different platforms, seasons, and instrument types. Our goal, rather, is to find patterns of performance among the different models to guide model improvement.

6. **Comparisons between Observations and Model results**

6.1 **Drill holes from coastal stations and Romanov Atlas.**

The residuals from the Romanov drill hole data were averaged from 1982 through 1986 and contoured using a color bar defined so that zero is white (Figure 4). All models, except for the GSFC model, show positive residuals, typically larger in the eastern Siberian marginal seas (East-Siberian and Chukchi Seas) than in the western seas (Kara and Laptev Seas).

6.2 **ICESat**

The residuals and correlations show that the models have a large scatter (Figure 5a). The UW, ECCO2, and NPS models are correlated with data above 0.6 and have residuals less than +0.30 m. For GSFC, the correlation is larger than 0.6 and the residual is negative, less than -0.40 m. The INMOM correlation is less than 0.5 and residual exceeds 0.40 m. (Post 2001 results from the ORCA model were not available at the time of our analysis.)

6.3 **Airborne EM**

The model and EM correlations are all less than 0.5. All models underestimate ice thickness except ECCO2 which has positive residuals (Figure 5b). Three models (GSFC, UW and NPS) demonstrate clustering of the results and have almost identical residuals, approximately -0.50 m. The negative residual occurs perhaps because the EM measurements include snow depth with the ice thickness although they underestimate maximum ridge thickness.

6.4 **Moored ULS**

All six models have similarly moderate correlations with residuals less than 0.25 m (Figure 5c). ECCO2, UW and GSFC have higher correlations with the data, near 0.6, while INMOM, NPS, and ORCA correlations are weaker. Of the six models, ECCO2 demonstrates the best agreement with the moored ULS data. Three models, INMOM, NPS and ORCA, show similar positive residuals. Two models, GSFC and UW, have negative, almost identical residuals.

6.5 **Submarine ULS**

ECCO2 has the highest correlation of ~0.7 in the suite of models with a residual of about +0.17 m (Figure 5d). UW, ECCO2 and GSFC models have similar correlations of about ~ 0.7. INMOM and NPS have positive residuals less than +0.70 m and correlations less than 0.6. ORCA has the weakest correlation (0.48) and a negative residual of approximately -0.30 m.

6.6 **Coastal stations and Romanov Atlas**

All models overestimate thickness at the coastal stations except for GSFC (Figure5e). The residuals are larger and more positive for the Romanov Atlas (symbols with squares in Figure 5e) except for GSFC which has a near zero residual for the station data and moderately negative residual for the Romanov Atlas data. NPS has the highest correlation with both the datasets although the residual for the Romanov Atlas data is large. GSFC shows the lowest correlation for the station data, whereas ORCA has the weakest for the Romanov Atlas data.

7. Basin-wide and regional model performance

We focus on model performance with respect to the ULS data because of (i) their broad spatial and temporal coverage, (ii) accuracy and biases of the measurements are relatively well understood, and (iii), like model grid-points, ULS measurements are values at a point sampled over time. The ULS data used here extend from 1990 through 2008 and cover the Beaufort Sea, Fram Strait and the Greenland Sea.

Figure 6 portrays correlations and residuals for the data from each model and from the individual moored ULS instruments. UW and ECCO2 show the smallest scatter of residuals (Figure 6 a,b). Residuals for GSFC and NPS are larger (Figure 6 c,d). The largest absolute residuals are from INMOM and ORCA with values approaching 2m (Figure 6 e,f). All models exhibit large scatter of the correlations; there is no apparent relationship between the scatter of the residuals and the correlations.

From Figure 6, the model performance clearly varies regionally. We next focus the analysis on Fram Strait and the Greenland Sea and on the Beaufort Sea. Figure 7 combines correlations and residuals for Fram Strait and the Greenland Sea (AWI moorings) and the Beaufort Sea (IOS and BGEP moorings) for all models. The pattern exhibits a broader range of residuals for the data acquired in Fram Strait/Greenland Sea compared to the Beaufort Sea. Typically the residuals for the Beaufort Gyre are more positive and higher than these for the periphery of the Beaufort Sea (Figure 7).

8. Linear relationships

The linear fit for the models and observations is shown in Figure 8 for a) satellite, b) airborne EM, c) moored ULS, d) submarine ULS, e) Coastal Stations and f) Romanov Atlas. Grey shading along the $y = x$ line indicates the accuracy of the measurements. In all but four cases, the y-intercepts are greater than zero indicating positive residuals for thin ice. In all but three cases the regression slopes are less than one. The regression lines cross y=x at variable locations with a mean of 2.2 m. For the satellite data (Figure 8a), INMOM, ECCO2, UW, and GSFC overestimate thickness where it is measured less than 1m. INMOM, ECCO2 and UW overestimate ice thinner than 2.0 - 2.5 m. NAME overlapped the satellite record only for 2004 and is omitted. For the airborne EM thicknesses (Figure 8b), all models strongly underestimate thickness when the ice is thicker than 3.5 m. ORCA is omitted as it does not have enough data for a meaningful comparison. For the moored ULS data (Figure 8c), GSFC strongly underestimates ice thinner than 2m and NPS, GSFC, and UW overestimate thin ice. All models except INMOM underestimate thick ice. For submarine ULS data (Figure 8d), all models overestimate thickness when measurements are less than 2 to 3 m. All models underestimate ice measured to be thicker than 4 m compared to submarine ULS.

Figure 8e shows that all models but NPS and GSFC overestimate near-shore ice thickness when measured to be less than 1.5 m at the Coastal Stations (Figure 8e). GSFC is unable to reproduce the range of the observed fast-ice measurements.

For the marginal seas (Romanov Atlas), INMOM, NPS, UW, and ORCA overestimate where observed thickness is less than 3 m, and all models overestimate thickness where it is measured to be less than 1 m (Figure 8f). (ECCO2 simulated 1992-2009 and does not overlap the Romanov Atlas data.)

9. Discussion

The accuracy, systematic errors of the measurements and cross-platform biases discussed in Section 4 should be taken into account when interpreting model results. Nevertheless, there are consistent results among the models.

For all observational platforms, most model regressions have slopes less than one ($\bar{m} = 0.7$), positive y-intercepts ($\bar{b} = 0.9$), and cross the y=x line (perfect fit) at a mean observed thicknesses of 2.1 m. The regressions indicate that thin ice is overestimated and thick ice is underestimated although each model varies around the 2.1 m mean crossing point (range -3.4 to 7.7). Overestimating thin ice is particularly evident with respect to the satellite data (Figure 8a). For the thickest ice (airborne EM and submarine ULS), which is generally the most deformed, all models underestimate thickness (Figure 8 a, b, d). There is thus a consistent pattern across platforms and across models to overestimate thin ice and underestimate thick ice. Below we investigate possible reasons for this bias.

The correlations are computed from multiple data sets that include different seasonal and spatial variability. For example, correlations should always be higher if the seasonal cycle is included compared to the correlations for just one season. This may explain why the modified Taylor diagrams suggest that the models perform well compared to the moored ULS (Figure 5).

Model performance is a clearly geographically dependent. Figures 5 and 6 demonstrate that the models as a group perform better in the Beaufort Sea than in other areas of the Arctic Ocean. The comparison with the IOS and BGEP moorings shows a smaller range of residuals than the other datasets. Scatter of the residuals for ULS measurements in Fram Strait and the Greenland Sea is larger than in the Beaufort Sea and substantial (Figure 7). Ice conditions in Fram Strait depend on local forcing as well as on conditions “upstream” in the Arctic Ocean making predictions for Fram Strait ice export dependent on many factors. However, the fact that the models do well in the central basin but not in Fram Strait and the Greenland Sea may suggest regional issues in Fram Strait are driving the poor performance there.

The poorest correlations are with the ice measured from the Airborne EM and the Romanov Atlas for the marginal Siberian seas. The residuals for the Airborne EM dataset are mostly negative and for the Romanov Atlas mostly positive and are larger than for the other data (Figure 5).

The models demonstrate reasonably good agreement with the coastal station data, which partly overlap the area of the Romanov Atlas measurements (Figures 5 and 8). The residuals for the coastal data have moderate scatter, however there is a positive bias of ~50 cm (Figure 5e). The bias may be because the station data represent only level sea ice whereas the model data are the cell-averaged level and ridge ice thicknesses. Note that AOMIP models do not have fast ice (motionless ice).

There are three aspects of the model biases. First, the biases tend to be smaller for the data which include several complete seasonal cycles (moored ULS and station data) and larger for the data covering only part of the year (satellite, Airborne EM, submarine ULS and Romanov Atlas). Since the latter mostly cover the ice melting period (spring to fall), we speculate that this may be related to model deficiencies in the thermodynamics of ice melting. The ice thickness threshold of 2.1 m, which in our analysis discriminates the positive and negative model bias, is the commonly accepted thickness distinguishing undeformed first- and multi-year Arctic sea ice [WMO, 1985]. This may indicate insufficient melting of first-year and the excessive melting of multi-year ice in the models. In our study we did not find any systematic differences between models with Semtner and energy-conserving thermodynamics.

The mean residual we found after averaging the annual residuals for the submarine ULS (Figure 5d) is 0.12 m. Recall that the submarine data were corrected for the 0.29 m bias reported by *Rothrock and Wensnahan* [2007]. As a group, the AOMIP models do well, overestimating submarine ULS by 0.12 m. We note that the Louvain-la-Neuve (LIM3) model [*Vancoppenolle et al.*, 2009a] underestimated submarine draft observations converted to thickness by -0.55±1.04. However, similar to our results, they obtained positive model bias for the thin ice and a negative bias for the thick ice. *Vancoppenolle et al.* [2009b] performed sensitivity study of ice thermodynamics to the sea ice salinity and demonstrated a 0.30 m reduction in the model bias when the salt evolution model is used instead of constant or prescribed varying salt profiles.

Second, the model biases indicate a regional dependency. Our analysis shows small residuals in the Beaufort Sea and the central Arctic Ocean (moored and submarine ULS data) and an increase of the positive residuals on the Siberian Shelf (station data and Romanov Atlas). *Rothrock et al.* [2003] and *Vancoppenolle et al.* [2009a], comparing model results with submarine ULS, obtained a persistent pattern of model biases with positive values in the Beaufort Sea, north of Greenland and towards the Alaskan and East-Siberian Shelves, and with negative values in the Arctic Transpolar Drift and towards Fram Strait. *Wilchinsky et al.* [2004] found a similar pattern in their simulations and demonstrated that using sliding friction in sea ice rheology can reduce the biases.

The third aspect is the interannual variability in the models and data. Given the errors in atmospheric temperature, humidity and radiation fields used to force the models, we would expect large model biases for individual years even though the overall long-term biases could be moderate. Most of the available Arctic ice thickness data represent a few "samples" per year when aggregated to a monthly time scale. This poses a large statistical uncertainty of the analysis. In addition, since the periods of the data collection varied from year to year, this introduces aliasing in the time series, making interpretation of the interannual variability difficult.

10. Summary

Sea ice thickness from six AOMIP coupled models is compared with thickness across the Arctic basin from a) satellites, b) airborne EM, c) moored ULS in Fram Strait, Greenland Sea and the Beaufort Gyre (ULS, IPS), d) submarine ULS across the central basin, and e) drill holes through fast along coastal Siberia and within the ice pack. The linear relationship between models and the different data shows that all models generally overestimates ice thinner than 2.1 m and underestimate the ice thicker than 4.0 m. This is a systematic error consistent among the models and is likely problematic for forecasting open water as well as in long term forecasts where the role of multi-year ice is critical. We speculate that this error may be attributed to the deficiencies in simulating ice melting. We did not find any systematic error with respect to the type of ice thermodynamics used in the models.

There is a significant scatter of the model biases with respect to the different observational platforms, which could be partly related to the observational systematic errors. The models agree best with the moored ULS data. The model skill in simulating sea ice thickness varies from region to region. Taken together, the models simulate the ice thickness in the Beaufort Gyre better than in Fram Strait and the Greenland Sea. Some of the observed scatter is also due to inconsistencies between different observational methods and data products. Averaging over all observational data sets, the correlations and smaller differences from observed thickness are better from the ECCO2 and UW models.

Acknowledgements

This research is supported by the National Science Foundation Office of Polar Programs covering awards of AOMIP collaborative research projects: ARC-0804180 (MJ), ARC-0804010 (AP), ARC-0805141 (WM), ARC080789 and ARC0908769 (JZ). Travel support to attend AOMIP meetings and publications fees for YA, IA, deCuevas, SH, RK, RL, and AN were provided by OPP project ARC-0804010. C. Haas is grateful for support with data acquisitions through the Alfred Wegener Institute in Germany and various EU projects. This research is also supported by the Russian Foundation of Basic Research, Projects 09-05-00266 and 09-05-01231. At the National Oceanography Centre Southampton this study was funded by the UK Natural Environment Research Council as a contribution to the Marine Centres' Strategic Research Programme Oceans2025. The NOCS-ORCA simulations were undertaken as part of the DRAKKAR collaboration [*Barnier et al*., 2006]. NOCS also acknowledges the use of UK National High Performance Computing Resource.

Reference list

Adcroft, A., and J.-M. Campin (2004), Rescaled height coordinates for accurate representation of free-surface flows in ocean circulation models, *Ocean Modelling*, *7* (3-4), 269--284.

Adcroft, A., C. Hill, and J. Marshall (1997), The representation of topography by shaved cells in a height coordinate model, *Mon. Weather Rev.,125* (9), 2293—2315.

Alexandrov, V., S. Sandven, J. Wahlin, and O. M. Johannessen (2010), The relation between sea ice thickness and freeboard in the Arctic, The Cryosphere, 4, 373–380, www.the-cryosphere.net/4/373/2010/ doi:10.5194/tc-4-373-2010.

Antonov, J.I., R.A. Locarnini, T.P. Boyer, A.V. Mishonov, and H.E. Garcia (2006), *World Ocean Atlas 2005*, chap. Volume 2: Salinity, p. 182pp, NOAA Atlas NESDIS 62, U.S. Government Printing Office, Washington, D.C.

Barnier B., Madec G., Penduff, T., Molines, J. M., Tréguier, A. M., Beckmann, A., Biastoch, A., Boning, C., Dengg, J., Gulev, S., Le Sommer, J., Rémy, E., Talandier, C., Theetten, S., Maltrud, M., Mc Lean, J. and B de Cuevas (2006), Impact of partial steps and momentum advection schemes in a global ocean circulation model at eddy permitting resolution. *Ocean Dyn.* 56, 543–567. DOI 10.1007/s10236-006-0082-1.

Bitz, C.M., J. Fyfe, and G. Flato (2002), Sea ice response to wind forcing from AMIP models, *J. Climate*, 15, 522-536

Blanke B. and P. Delecluse (1993), Variability of the tropical Atlantic Ocean simulated by a general circulation model with two different mixed-layer physics. *J. Phys. Oceanogr*. 23, 1363-1388.

Blumberg A., and G. L. Mellor, (1987), A description of a three-dimensional coastal ocean circulation model. In Three-Dimensional Coastal Ocean Models, N. S. Heaps (Ed.), 1-16, American Geophysical Union, Washington, DC

Bourke, R. H., and R. P. Garrett (1987), Sea ice thickness distribution in the Arctic Ocean, Cold Reg. Sci. Technol., 13(3), 259 – 280.

Bourke, R. H., and R. G. Paquette (1989), Estimating the thickness of sea ice, J. Geophys. Res., 94, 919 – 923

Brodeau L., Barnier B., Penduff T., Treguier A.M. and S. Gulev (2001), An ERA-40 based atmospheric forcing for global ocean circulation models. *Ocean Modelling,* 31, 88-104.

Brydon D., S. San, R. Bleck (1999), A new approximation of the equation of state for seawater, suitable for numerical ocean models. *J. Geophys. Res*.104, C1., 1537-1540.

Dai A., and K.E. Trenberth (2002), Estimates of freshwater discharge from continents: latitudinal and seasonal variations. *Journal of hydrometeorology*, 3, 660-687.

Daru, V., and C. Tenaud (2004), High order one-step monotonicity-preserving schemes for unsteady compressible flow calculations, *J. Comput. Phys*., 193 (2), 563--594, doi{http://dx.doi.org/10.1016/j.jcp.2003.08.023}.

Eicken, H., W.B. Tucker III, D.K. Perovich (2001), Indirect measurements of the mass balance of summer Arctic sea ice with an electromagnetic induction technique, *Ann.Glaciol*., 33, 194-200.

Fichefet T. and M. A. Morales Maqueda (1997), Sensitivity of a global sea ice model to the treatment of ice thermodynamics and dynamics. *J. Geophys. Res.* 102, 12609-12646.

Flato, G.M. and CMIP contributors (2004), Sea-ice climate and sensitivity as simulated by global climate models, *Climate Dynamics*, 23: 229-241

Flato G.M., Hibler, W.D. III (1995), Ridging and strength in modeling the thickness distribution of Arctic sea ice. *J. Geophys Res.*, 100:18,611–18,626.

Fox-Kemper, B., and D. Menemenlis (2008), Can large eddy simulation techniques improve mesoscale rich ocean models?, in *Ocean Modeling in an Eddying Regime*, edited by M. Hecht and H. Hasumi, pp. 319--338, AGU, Washington, D.C.

Gaspar P., Grégoris Y. and J. M. Lefevre (1990), A simple eddy-kinetic-energy model for simulations of the ocean vertical mixing: tests at station Papa and long-term upper ocean study site. *J. Geophys. Res.* 95, 16,179-16,193.

Gerdes, R., and C. Köberle (2007), Comparison of Arctic sea ice thickness variability in IPCC Climate of the 20th Century experiments and in ocean–sea ice hindcasts, *J. Geophys. Res.*, *112*, C04S13, doi:10.1029/2006JC003616

Gloersen, P., Campbell, W. J., Cavalieri, D. J., Comiso, J. C., Parkinson, C. L., and Zwally, H. J. (1992), Arctic and Antarctic sea ice, 1978-1987: Satellite passive-microwave observations and analysis: Washington, NASA Scientific and Technical Information Program SP-511, 290 p.

Haas, C., and P. Jochmann (2003), Continuous EM and ULS thickness profiling in support of ice force measurements. In Proceedings of the 17th International Conference on Port and Ocean Engineering under Arctic Conditions, POAC ´03, Trondheim, Norway, vol. 2, edited by S. Loeset, B. Bonnemaire, and M. Bjerkas, pp. 849–856, Department of Civil and Transport Engineering, Norwegian University of Science and Technology NTNU, Trondheim, Norway.

Haas, C., S. Gerland, H. Eicken, and H. Miller (1997), Comparison of sea-ice thickness measurements under summer and winter conditions in the Arctic using a small electromagnetic induction device. *Geophysics*, 62(3), 749–757.

Haas, C., Hendricks, S., Doble, M.(2006), Comparison of the sea ice thickness distribution in the Lincoln Sea and adjacent Arctic Ocean in 2004 and 2005, Annals of glaciology,44, 247-252.

Haas, C., S. Hendricks, H. Eicken, and A. Herber (2010), Synoptic airborne thickness surveys reveal state of Arctic sea ice cover, *Geophys. Res. Lett*., 37, L09501, doi:10.1029/2010GL042652.

Haas, C., J. Lobach, S. Hendricks, L. Rabenstein, and A. Pfaffling (2009), Helicopter-borne measurements of sea ice thickness, using a small and lightweight, digital EM system, *J. Appl. Geoph.*, 67(3), 234–241, 2009, doi:10.1016/j.jappgeo.2008.05.005.

Haas, C., A. Pfaffling, S. Hendricks, L. Rabenstein, J.-L. Etienne, and I. Rigor (2008), Reduced ice thickness in Arctic Transpolar Drift favors rapid ice retreat, *Geophys. Res. Lett.*, 35, L17501, doi:10.1029/2008GL034457.

Hakkinen, S. and C.A. Geiger (2000), Simulated low frequency modes of circulation in the Arctic Ocean, *J. Geophys. Res.*, 105, 6549-6564.

Hakkinen, S., and G. L. Mellor (1992), Modeling the seasonal variability of the coupled Arctic ice-ocean system, J. Geophys. Res., 97, 20,285 –20,304

Hibler, W.D., III (1979), A dynamic thermodynamic sea ice model. *J. Phys. Oceanogr.* 9, 815-846.

Hibler, W. D., (1980), Modeling a Variable Thickness Sea Ice Cover. *Mon. Wea. Rev.*, **108**, 1943-1973. doi: 10.1175/1520-0493

Hibler, W. D., and K. Bryan (1987), A Diagnostic Ice Ocean Model, *J.Phys. Oceanogr.*, *17*, 987-1015.

Holland, D.M. (2000), Merged IBCAO/ETOPO5 Global Topographic Data Product. National Geophysical Data Center (NGDC), Boulder CO.

Holland, D., Holloway,G., F. E.Dupont. E.Golubeva, S.Ha¨kkinen, E.Hunke, M.Jin, M.Karcher, F.Kauker, M.Maltrud, M.A.Morales Maqueda,W.Maslowski, G.Platov, D.Stark, M.Steele, T.Suzuki, J.Wang, and J.Zhang (2007), *J. Geophys. Res.*, v.112, C04S03, doi: 10.1029/2006JC003642.

Hunke, E. C. (2001), Viscous-plastic sea ice dynamics with the evp model: Linearization issues. *J. Comp. Phys.*, **170**, 18-38.

Hunke, E.C. and C.M. Bitz (2009), Age characteristics in a multidecadal arctic sea ice simulation. *J.Geophys.Res.*, 114, C08013, doi:10.1029/2008JC005186.

Hunke, E., and M. Holland (2007), Global atmospheric forcing data for Arctic ice-ocean modeling, *J.Geophys. Res.*, 112, C06S14, doi:10.1029/2006JC003.

Jackett, D. R., and T. J. McDougall (1995), Minimal adjustment of hydrographic profiles to achieve static stability, *J. Atmos. Oceanic Technol.*, *12* (2), 381—389.

Johnson, M., S. Gaffigan, E. Hunke, and R. Gerdes (2007), A comparison of Arctic Ocean sea ice concentration among the coordinated AOMIP model experiments, *J. Geophys. Res.*, *112*, C04S11, doi:10.1029/2006JC003690.

Kalnay, E., M. Kanamitsu, R. Kistler, W. Collins, D. Deaven, L. Gandin, M. Iredell, S. Saha, G. White, J. Woollen, Y. Zhu, M. Chelliah, W. Ebisuzaki, W.Higgins, J. Janowiak, K. C. Mo, C. Ropelewski, J. Wang, A. Leetmaa, R. Reynolds, Roy Jenne, Dennis Joseph (1996). The NCEP/NCAR 40-Year Reanalysis Project. *Bulletin of the American Meteorological Society* **77** (3): 437–471

Kochergin V. P. (1987), Three-Dimensional Prognostic Models, in *Coastal Ocean Models*, Ed. by N. Heaps (AGU, Coastal and Estuarine Science, Vol. 4, 841–849.

Konstantinov, Yu. B., K. I. Grachev. 2000. *High-latitude Airborne Expeditions Sever (1937, 1941 – 1993)*. Gidrometeoizdat Publishing House, St. Petersburg, Russia, 176 pp

Kwok, R., and D.A. Rothrock (2009), Decline in Arctic sea ice thickness from submarine and ICESat records: 1958:2008. Geophys. Res. Lett., V. 36, L15501, doi:10.1029/2009GL039035, 2009

Kwok, R., G. F. Cunningham, M. Wensnahan, I. Rigor, H. J. Zwally, and D. Yi (2009), Thinning and volume loss of the Arctic Ocean sea ice cover: 2003 – 2008, J. Geophys. Res., 114, C07005, doi:10.1029/2009JC00531

Kwok, R., G. F. Cunningham, H. J. Zwally, and D. Yi (2007), Ice, Cloud, and land Elevation Satellite (ICESat) over Arctic sea ice: Retrieval of freeboard, *J. Geophys. Res.*, 112, C12013, doi:10.1029/2006JC003978

Kwok, R., E. Hunke, W. Maslowski, D. Menemenlis, and J. Zhang (2008), Variability of sea ice simulations assessed with RGPS kinematics. *J. Geophys. Res.*, 131, C11012.

Kwok, R., H. J. Zwally, and D. Yi (2004), ICESat observations of Arctic sea ice: A first look. *Geophys. Res. Lett.*, 31, L16401, doi:10.1029/2004GL020309.

Large W. G. and S.G. Yeager (2004), Diurnal to decadal global forcing for ocean and sea-ice models: The data sets and flux climatologies. NCAR technical note: NCAR/TN-460+STR, NCAR, 105pp.

Large, W. G., J. C. McWilliams, and S. C. Doney (1994), Oceanic vertical mixing: a review and a model with nonlocal boundary layer parameterisation, *Rev. Geophys.*, *32*, 363-403.

Laxon, S., N. Peacock, and D. Smith (2003), High interannual variability of sea ice thickness in the Arctic region, *Nature*, 425, 947 – 950.

Leith, C. E. (1996), Stochastic models of chaotic systems, *Physica D*, *98*, 481—491.

Lévy M., Estublier A. and G. Madec (2001), Choice of an advection scheme for biogeochemical models. *Geophys Res Lett.* 28, 3725–3728. DOI 10.1029/2001GL012947.

Lindsay, R. W. (2010), Unified Sea Ice Thickness Climate Data Record, Polar Science Center, Applied Physics Laboratory, University of Washington, psc.apl.washington.edu/sea_ice_cdr, digital media.

Locarnini, R. A., A. V. Mishonov, J. I. Antonov, T. P. Boyer, and H. E. Garcia (2006), *World Ocean Atlas 2005*, chap. Volume 1: Temperature, 182pp, NOAA Atlas NESDIS 62, U.S. Government Printing Office, Washington, D.C.

Losch, M., D. Menemenlis, P. Heimbach, J.-M. Campin, and C. Hill (2010), On the formulation of sea-ice models. part 1: effects of different solver implementations and parameterizations, *Ocean Modelling*, *33*, 129—144.

Madec, G. (2006), NEMO reference manual, ocean dynamics component: NEMO-OPA. Preliminary version. Note du Pole de modélisation, Institut Pierre-Simon Laplace (IPSL), France, 27, ISSN No. 1288-1619.

Marshall, J., A. Adcroft, C. Hill, L. Perelman, and C. Heisey (1997), A finite-volume, incompressible Navier-Stokes model for studies of the ocean on parallel computers, *J. Geophys. Res.*, *102* (C3), 5753—5766.

Maslowski, W., and W. Lipscomb (2003), High resolution simulations of Arctic sea ice, 1979 – 1993, Polar Res., 22, 67 – 74

Maslowski, W., J. Clement Kinney, D. C. Marble, J. Jakacki, (2008) In: Ocean Modeling in an Eddying Regime, M. W. Hecht and H. Hasumi, eds. Geophysical Monograph Series, Volume 177, 350 pp.

Maslowski, W., D. Marble, W. Walczowski, U. Schauer, J. L. Clement, and A. J. Semtner (2004), On climatological mass, heat, and salt transports through the Barents Sea and Fram Strait from a pan-Arctic coupled ice-ocean model simulation, *J. Geophys. Res.*,*109*, C03032, doi:10.1029/2001JC001039.

Maslowski, W., B. Newton, P. Schlosser, A. Semtner, and D. Martinson (2000), Modeling recent climate variability in the Arctic Ocean, *Geophys. Res. Lett.*, 27, 3743 – 3746

Melling, H., and D.A.Riedel (2004), Draft and movement of pack ice in the Beaufort Sea: a time-series presentation April 1990 – August 1999. Canadian Technical Report of Hydrography and Ocean Sciences 238. 331pps.

Melling, H., and D.A. Riedel (2008), Ice Draft and Ice Velocity Data in the Beaufort Sea, 1990-2003. Boulder, Colorado USA: National Snow and Ice Data Center. Digital media.

Mellor, G.L, S. Hakkinen, T. Ezer, and R. Pazan, (2002), A generalization of a sigma coordinate ocean model and an intercomparison of model vertical grids, in 'Ocean Forecasting: Theory and Practice', N. Pinardi and J.D.Woods, eds., Springer-Verlag, 55-72. Pub.

Mellor, G.L. and L.H. Kantha (1989), An ice-ocean coupled model, *J. Geophys. Res*., 94, 10937-10954.

Mellor, G.M. and T. Yamada (1974), A hierarchy of turbulence closure models for planetary boundary layer, *J. Atmas. Sci*., 31, 1791-1806.

Mellor, G.L. and T. Yamada (1982), Development of a turbulence closure model for geophysical fluid problems, *Rev. Geophys*., 20, 851-875.

Menemenlis, D., J.M. Campin, P. Heimbach, C. Hill, T. Lee, A. Nguyen, M. Schodlok, H. Zhang (2008), ECCO2: High resolution global ocean and sea ice data synthesis, *Mercator Ocean Quarterly Newsletter*, *31*, 13—21.

Moshonkin S.N., G.V. Alekseev, A.V. Bagno, A.V. Gusev, N.A. Diansky, and V.B. Zalesny (2011), Numerical modeling of the 20th century variability of the North Atlantic-Arctic Ocean-Bering Sea circulation. *Russian Journal of Numerical Analysis and Mathematical Modelling*. Vol. 26, Issue 2, (in press).

Nguyen, A. T., D. Menemenlis, and R. Kwok (2009), Improved modeling of the Arctic halocline with a subgrid-scale brine rejection parameterization, *J. Geophys. Res.*, *114*, C11014.

Nguyen, A.T., D. Menemenlis, and R.Kwok (2011), Arctic ice-ocean simulation with optimized model parameters: approach and assessment. *J. Geophys. Res.* (in press)

Onogi, K., J. Tsutsui, H. Koide, M. Sakamoto, S. Kobayashi, H. Hatsushika, T.Matsumoto, N.Yamazaki, H. Kamahori, K. Takahashi, S. Kadokura, K. Wada, K. Kato, R. Oyama, N. M. T. Ose, and R. Taira (2007), The jra-25 reanalysis, *J. Meteor. Soc. Japan, 85* (3), 369—43.

Pacanowski, R.C., and A. Gnanadesikan (1998), Transient response in a Z-level ocean model that resolves topography with partial cells, *Monthly Weather Review*, 126, 3248-3270.

Parkinson, C. L., and W. M. Washington (1979), A large scale numerical model of sea ice, *J. Geophys.Res. 84*, 311-337.

Payne, R.E. (1972), Albedo of the sea surface. *J. Atmos. Sci.*, 29, 959-970.

Penduff, T., J. Le Sommer, B. Barnier, A.-M. Treguier, J.-M. Molines, and G. Madec (2007), Influence of numerical schemes on current-topography interactions in 1/4° global ocean simulations, *Ocean Sci.*, 3, 509-524.

Rodrigues, J. (2011), Beamwidth effects on sea ice draft measurements from U.K. submarines, Cold Regions science and Techn., 65, 160-171.

Semtner, A.J. (1976), A model for the thermodynamic growth of sea ice in numerical investigation of climate. *J. Phys. Oceanogr.* 6, 376-389.

Pfaffling, A., C. Haas, and J. Reid (2007), A direct helicopter EM sea ice thickness inversion, assessed with synthetic and field data, *Geophysics*, 72, F127-F137.

Prather, M.C. (1986), Numerical advection by conservation of second-order moments. *J. Geophys. Res.* 91, 6671-6681.

Rasmusson, E.M. and K. Mo (1996) Large scale atmospheric moisture cycling as evaluated from NMC global analysis and forecast products, *J. Climate*, 9, 3276-3297.

Reid, J. E., A. Pfaffling, J. Vrbancich (2006), Airborne electromagnetic footprints in 1D earths, *Geophysics*, 71(2), G63-G72, doi:10.1190/1.2187756.

Romanov, I.P. (1995), In: Tunik, A. (Ed.), Atlas of Ice and Snow of the Arctic Basin and Siberian Shelf Seas. Backbone Publishing Company. 277 pp.

Rothrock, D. A., and M. Wensnahan (2007), The accuracy of sea ice drafts measured from U.S. Navy submarines, J. Atmos. Oceanic Technol., 24, 1936– 1949, doi:10.1175/JTECH2097.1.

Rothrock, D. A., Y. Yu, and G. A. Maykut (1999), Thinning of the Arctic sea-ice cover, *Geophys. Res. Lett.*, 26(23), 3469 – 3472, doi:10.1029/1999GL010863.

Rothrock, D. A., D. B. Percival, and M. Wensnahan (2008), The decline in arctic sea-ice thickness: Separating the spatial, annual, and interannual variability in a quarter century of submarine data, *J. Geophys. Res.*, 113, C05003, doi:10.1029/2007JC004252.

Rothrock, D. A., J. Zhang, and Y. Yu (2003), The arctic ice thickness anomaly of the 1990s: A consistent view from observations and models, *J. Geophys. Res*., 108(C3), 3083, doi:10.1029/2001JC001208.

Semtner, A.J. (1976), A model for the thermodynamic growth of sea ice in numerical investigation of climate. *J. Phys. Oceanogr*. 6, 376-389.

Smith, R.D., J. K. Dukowicz, and R. C. Malone, (1992), Parallel ocean general circulation modeling. *Physica D*, 60, 30–6.

Smith, R.D. and P. R. Gent, Eds., (2002), Reference manual for the Parallel Ocean Program (POP): Ocean component of the Community Climate System Model (CCSM2.0 and 3.0).

Smith, W. H. F., and D. T. Sandwell (1997), Global sea floor topography from satellite altimetry and ship depth soundings, *Science*, *277* (5334), 1956—1962.

Steele, M., et al. (2001), PHC: A global ocean hydrography with a highquality Arctic Ocean, J. Clim., 14, 2079 – 2087

Steffen, K. (ed.) (2004), Workshop on Sea-Ice Thickness Measurements from Moored Ice-Profiling Sonars: Calibration, Data Processing and Application, Arctic Climate System Study and Climate and Croyosphere Project, Informal Report No. 15/2004.

Taylor, K. E. (2001), Summarizing multiple aspects of model performance in a single diagram, *J. Geophys. Res*., 106(D7), 7183-7192

Thorndike, A. S., D. S. Rothrock, G. A. Maykut and R. Colony (1975), The thickness distribution of sea ice. *J. Geophys. Res.*, **80**, 4501-4513

Timmermann, R., H. Goose, G. Madec, T. Fichefet, C. Ethe, and V. Duliere (2005), On the representation of high latitude processes in the ORCA-LIM global coupled sea ice-ocean model, *Ocean Model.*, 8, 175–201.

Untersteiner, N. (1961), On the mass and heat budget of Arctic sea ice, *Arch. Meteor. Geophys. Bioklimatol., Ser. A*. 12. 151-182.

Vancoppenolle M., T. Fichefet and H. Goosse (2009), Simulating the mass balance and salinity of Arctic and Antarctic sea ice.2. Sensitivity to the ice salinity processes Ocean Modelling 27, 54-69.

Vancoppenolle, M., T. Fichefet, H. Goosse, S. Bouillon, G. Madec, and M. A. Morales Maqueda (2009a), Simulating the mass balance and salinity of Arctic and Antarctic sea ice. 1. Model description and validation, *Ocean Modelling*, *27 (1–2)*, 33–53, doi:doi:10.1016/j.ocemod.2008.10.005.

Volodin E. M., N. A. Dianskii, and A. V. Gusev (2010), Simulating Present-Day Climate with the INMCM4.0 Coupled Model of the Atmospheric and Oceanic General Circulations. Izvestiya, *Atmospheric and Oceanic Physics,* ISSN 0001-4338. Vol. 46, No. 4, 2010. 414-431.

Wadhams, P. (1990), Evidence for thinning of the Arctic ice cover north of Greenland, *Nature,* 345,795-797.

Wadhams, P., and N. R. Davis (2000), Further evidence of ice thinning in the Arctic Ocean, *Geophys. Res. Lett.*, *27*(24), 3973–3975, doi:10.1029/2000GL011802

Walsh, J.E., Crane, R.G. (1992), A comparison of GCM simulations of Arctic climate. *Geophys. Res. Lett.* 19, 29–32

Wilchinsky, A.V., and D.L.Feltham (2004), Dependence of sea ice yield-curve shape on ice thickness. *J.Phys.Ocean*., 34, 2852-2856.

Winsor, P. (2001), Arctic sea ice thickness remained constant during the 1990s, *Geophys. Res. Lett.*, 28(6), 1039 – 1041

Witte, H., and E. Fahrbach (2005), AWI moored ULS data, Greenland Sea and Fram Strait, 1991-2002. Boulder, CO: National Snow and Ice Data Center/World Data Center for Glaciology. Digital media.

World Meteorological Organization (1985), WMO sea-ice nomenclature, terminology, codes and illustrated glossary, WMO/DMM/BMO 259-TP-145, Secretariat of the WMO, Geneva.

Yaglom, A.M. and B.A.Kader (1974), Heat and mass transfer between a rough wall and turbulent flow at high Reynolds and Pcelet numbers, *J.Fluid Mech*., 62, 601-623.

Yakovlev N.G. (2009), Reproduction of the Large-Scale State of Water and Sea Ice in the Arctic Ocean in 1948–2002: Part I. Numerical Model. Izvestiya, *Atmospheric and Oceanic Physics*, ISSN 0001-4338. Vol. 45, No. 3, 2009, 357-371.

Zhang, J. (2005), Warming of the arctic ice-ocean system is faster than the global average since the 1960s, *Geophys. Res. Lett.*, *32.*

Zhang, J. and W.D. Hibler (1997), On an efficient numerical method for modeling sea ice dynamics, *J. Geophys. Res.*, *102*, 8691–8702.

Zhang, J., and M. Steele (2007),, The effect of vertical mixing on the Atlantic water layer circulation in the Arctic Ocean, J. Geophys. Res.,112, C04S04, doi:10.1029/2006JC003732.

Zhang, J., and D. Rothrock (2001), A thickness and enthalpy distribution sea-ice model, *J.Phys. Oceanogr.*, *31*, 2986-3001.

Zhang, J., and D.A. Rothrock (2003), Modeling global sea ice with a thickness and enthalpy distribution model in generalized curvilinear coordinates, *Mon. Wea. Rev*., *131(5)*, 681–697.

Zhang, J., and D.A. Rothrock (2005), The effect of sea-ice rheology in numerical investigations of climate, *J. Geophys. Res., 110*, C08014, doi:10.1029/2004JC002599.

Zhang, Y., W. Maslowski, and A.J. Semtner (1999), Impact of mesoscale ocean currents on sea ice in high resolution Arctic ice and ocean simulations, *J. Geophys. Res*., 104(C8), 18,409-18,430.

Figure Captions

Figure 1. (a) ICESat data extent for the February-March and October-December 2004 – 2008 campaigns. (b) Locations of ULS in Fram Strait and the Greenland Sea (AWI, red), Beaufort Sea (BGEP, blue; IOS, green), Romanov (1995) landing data from subset of High-Latitude Airborne Annual (Sever) Expeditions (dark red dots), and 51 coastal fast ice stations (dark grey).

Figure 2. Locations of the airborne EM thickness data (dark) and submarine ULS ice draft data (light).

Figure 3. Taylor diagram modified so the correlation coefficient is the radial distance from the center. The rotation angle is proportional to the residual (model minus observed thickness) where ± 2 m rotates to $\pm\pi$ with larger residuals rotated away from the positive x-axis. A correlation coefficient of 0.6 is marked by the dashed green circle and residuals of 30 and 75 cm are marked.

Figure 4. Residual sea ice thickness from the Romanov Atlas data (stations in Figure 1) from 1982 through 1986 for (a) UW, (b) NPS, (c) GSFC, (d) INMOM, and (e) ORCA. No ECCO2 model results overlap with the Romanov data. Blue color identifies where model overestimates thickness (UW, NPS, INMOM, ORCA) and red color denotes underestimate (GSFC).

Figure 5. Correlations and residuals for models and (a) ICESat, (b) airborne EM, (c) moored ULS (d) submarine ULS, (e) 51 coastal stations and Romanov Atlas (with squares).

Figure 6. Correlations and residuals for moored ULS data. UW and ECCO2 have smaller residuals compared to other models. GSFC and NPS have larger residuals. INMOM and ORCA have the largest residuals with some approaching 2 m. AWI instrument data are in red, IOS in green, and BGEP in blue.

Figure 7. Correlations and residuals for moored ULS data from (a) Fram Strait and the Greenland Sea (AWI) and (b) Beaufort Sea (IOS, BGEP). The models simulate better the data from the Beaufort Sea compared to Fram Strait and the Greenland Sea. Colors identifying each model are the same as in Figure 6.

Figure 8. Linear fit between observed and model thickness from (a) satellites, (b) airborne EM, (c) moored ULS, (d) submarine ULS, (e) coastal stations, and (f) Romanov Atlas. Each axis limit is set from the maximum observed using the particular platform. Measurement accuracy is shown by the width of the grey area behind the black $y = x$ line. A width of 10 cm is used for the coastal station data and Romanov Atlas.

Tables

Table 1. Model Configuration and Selected Parameters[a]

	GSFC	ECCO2	INMOM	NOCS	NAME	UW
Domain	regional	regional	regional	global	regional	regional
Resolution	0.35º - 045º	15-22km	0.25º	3-6 km	9 km	6-75 km
Ice Δt	720 s	600 s	3600 s	7200 s	2800s	1152 s
Vertical coordinate	z	z	σ	z	z	z
Vertical levels	26	50	27	64	45	30
Minimum depth	25m	5m	5m	6.06	10	5m
Bering Strait	Restored	Not restored	open	Fully represented in global domain	open	open
Equation of state	Mellor	Jackett and McDougal, 1995	Brydon et al., 1999	Jackett & McDougall (1995)	UNESCO	UNESCO
Vertical	MY2.5	KPP, no	Monin and	TKE	Pacanowsk	KPP

mixing		double diffusion	Obukhov, (Kochergin, 1987)	(Gaspar *et al*.(1990), Blanke & Delecluse (1993))	i and Philander	
Tracer advection	Lin et al 1994 Piecewise parabolic	7th order monotonicity-preserving (Direct space time with flux limiter) [Daru and Tenaud, 2004]	Central diff.	TVD (Lévy *et al*. 2001)	Central diff.	Central diff.
Momentum advection	centered	vector invariant	Central diff.	EEN (Barnier *et al*. 2006)	Central diff.	Central diff.
Salinity	5	Function of surface S	4	6	4	4
Thickness categories[d]	2: ice and no ice	8 (7 for ice and 1 for open water)	1	1	2: mean grid cell ice thickness	12

					or open water	
Advection	Centered mom. Upwind A+D	Centered 2nd order	MPDATA	Prather, 2nd order, 2nd moment conserving	Central diff.	Central diff.
Dynamics[e]	Generalized viscous	Viscous plastic	EVP	VP	Viscous plastic	Teardrop plastic rheology, LSR solver
Albedos						
Melting snow	Cold snow - 0.85 0.78 – melting snow	0.8085	0.7-0.8 (surface temperature dependent)	0.5-0.65 (clear sky, snow thickness dependent)		0.70
Cold ice	0.74	0.7	0.1-0.65 (ice thickness dependent)	0.1-0.72 (clear sky, ice thickness dependent)	0.73	0.75

Melting ice	0.7	0.7060	0.1-0.575 (ice thickness and surface temperature dependent)	01.-0.5 (clear sky, ice thickness dependent)		0.64
Ocean	0.1	0.1556	0.1	0.06	.10	0.1
Surface Momentum Exchange Coefficients						
Atmos.-ice[g]	1.4E-3	1.14 x 10^-3	2.75 x 10^{-3}	1.63 x 10^{-3}	1.1 x 10^{-3}	Surface BL
Ice-Ocean	BL model	5.4 x 10^-3	5.5 x 10^{-3}	5.0 x 10^{-3}	5.5 x 10^{-3}	Cw=0.0055

[a]See AOMIP web site for additional details (http://www.whoi.edu/AOMIP)

Table 2. ICESat campaign periods

Laser	Campaign year	Period	Operational Days
2a	2003	Sep 24 – Nov18	55
2b	2004	Feb 17 - Mar 21	34
3a	2004	Oct 03 – Nov 08	37
3b	2005	Feb 17 – Mar 24	36
3d	2005	Oct 21 – Nov 24	35
3e	2006	Feb 22 – Mar 27	34
3g	2006	Oct 25 – Nov 27	34
3h	2007	Mar 12 – Apr 14	34
3i	2007	Oct 02 – Nov 05	37
3j	2008	Feb 17 – Mar 21	34

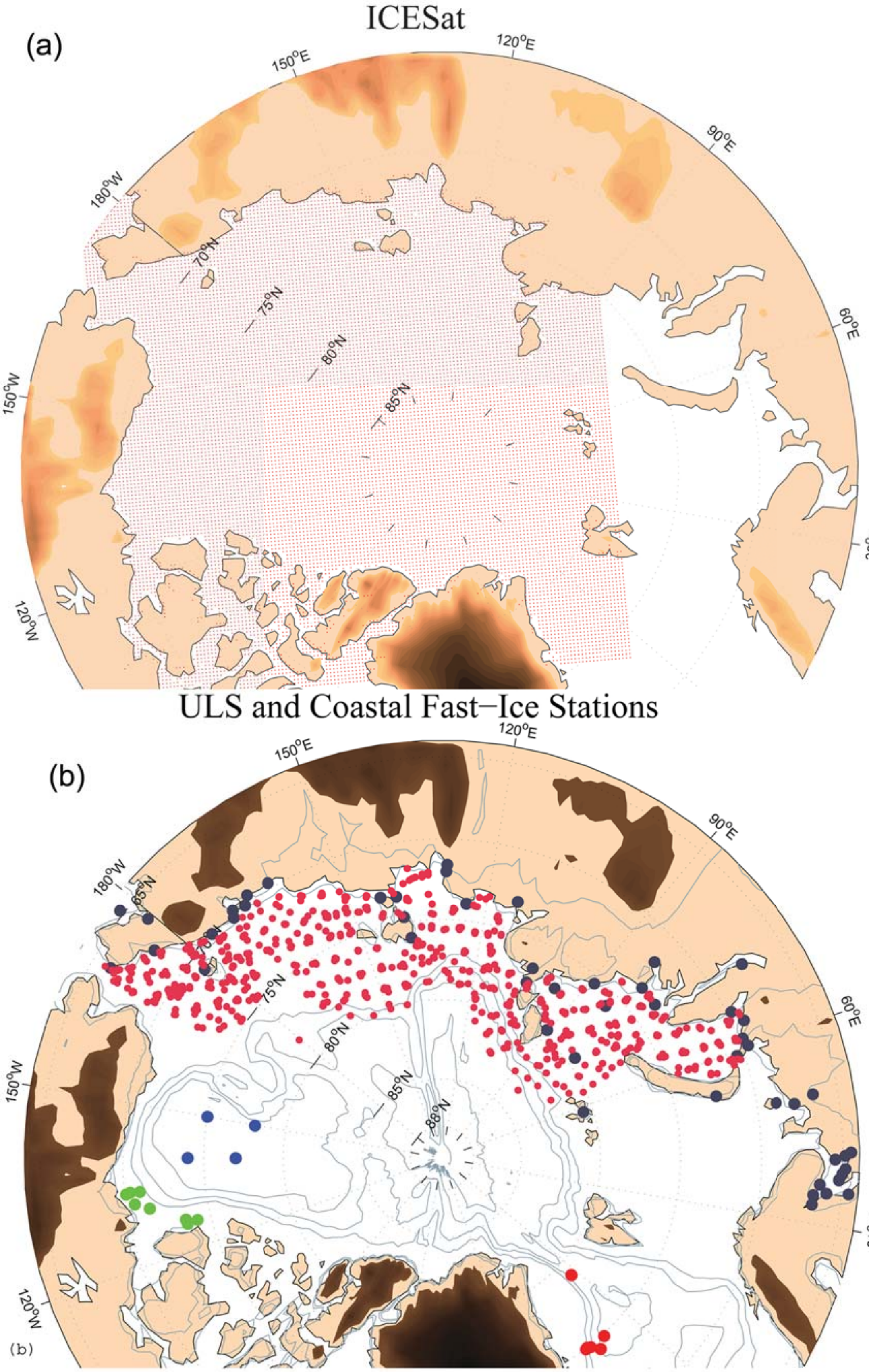

ICESat
(a)
120°E
150°E
90°E
180°W
70°N
75°N
80°N
85°N
60°E
150°W
30°E
120°W
ULS and Coastal Fast−Ice Stations
(b)
120°E
150°E
90°E
180°W
65°N
75°N
80°N
85°N
88°N
60°E
150°W
30°E
120°W
(b)

Figure 1

Submarine and Airborne EM Stations

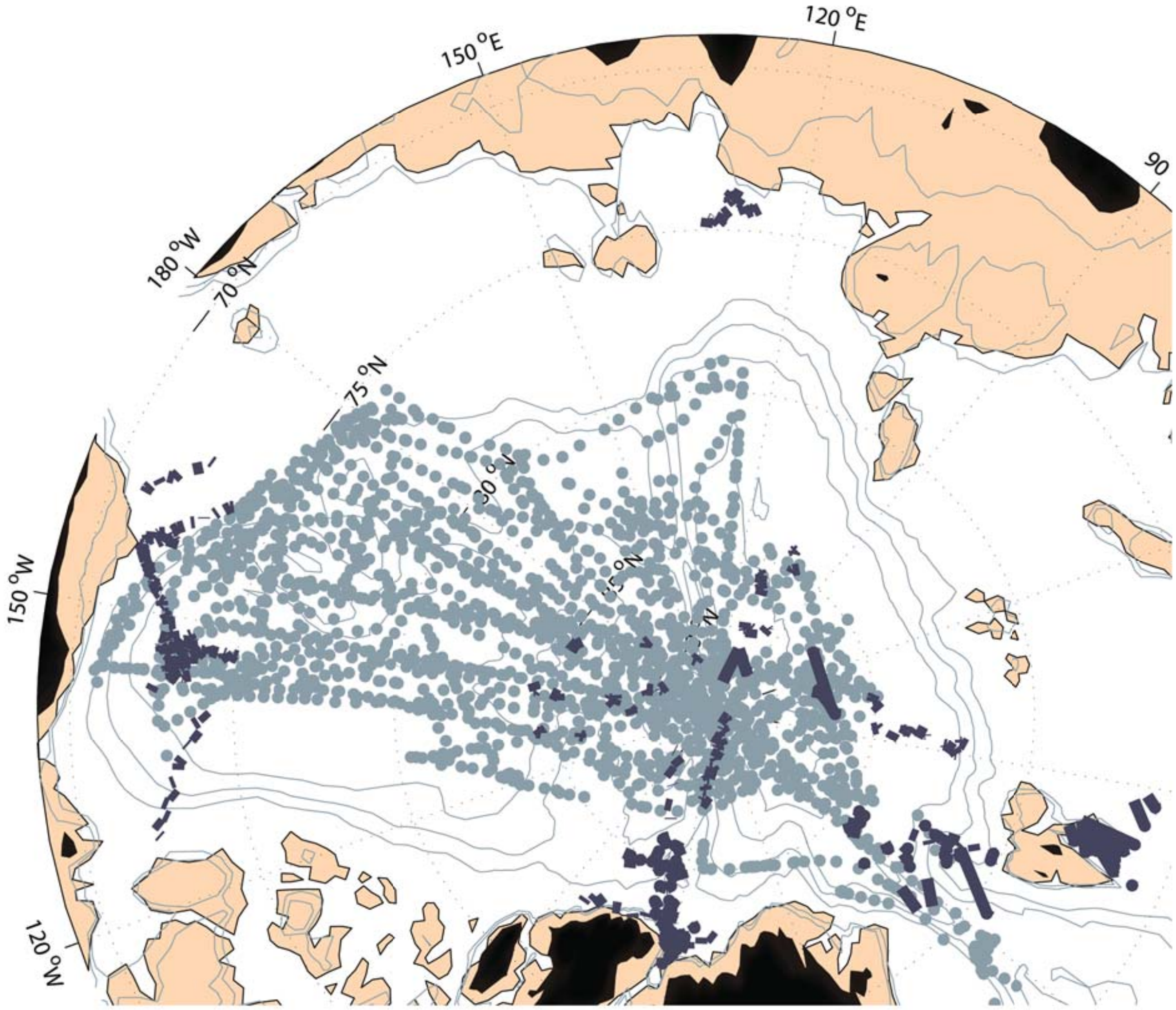

Figure 2

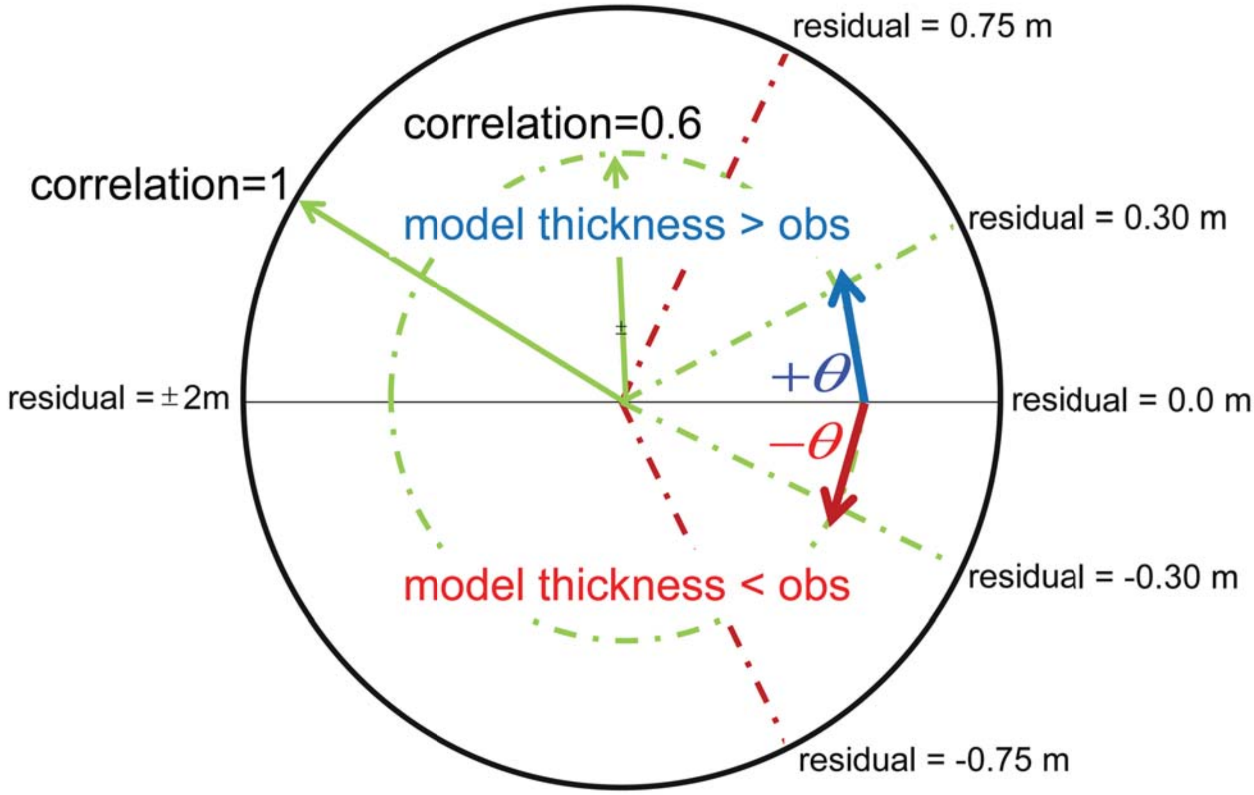
residual = 0.75 m
correlation=0.6
correlation=1
model thickness > obs
residual = 0.30 m
+θ
residual = ±2m
residual = 0.0 m
−θ
residual = -0.30 m
model thickness < obs
residual = -0.75 m

Figure 3

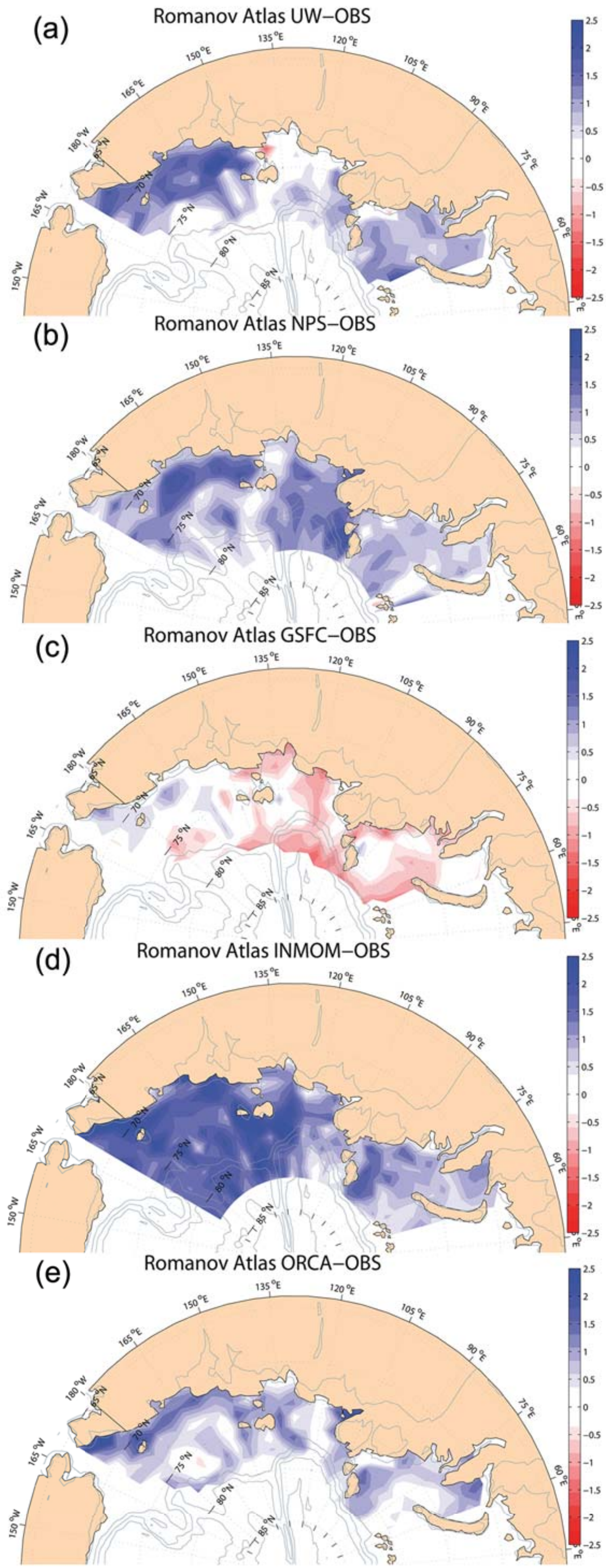
(a)
Romanov Atlas UW–OBS
(b)
Romanov Atlas NPS–OBS
(c)
Romanov Atlas GSFC–OBS
(d)
Romanov Atlas INMOM–OBS
(e)
Romanov Atlas ORCA–OBS

Figure 4

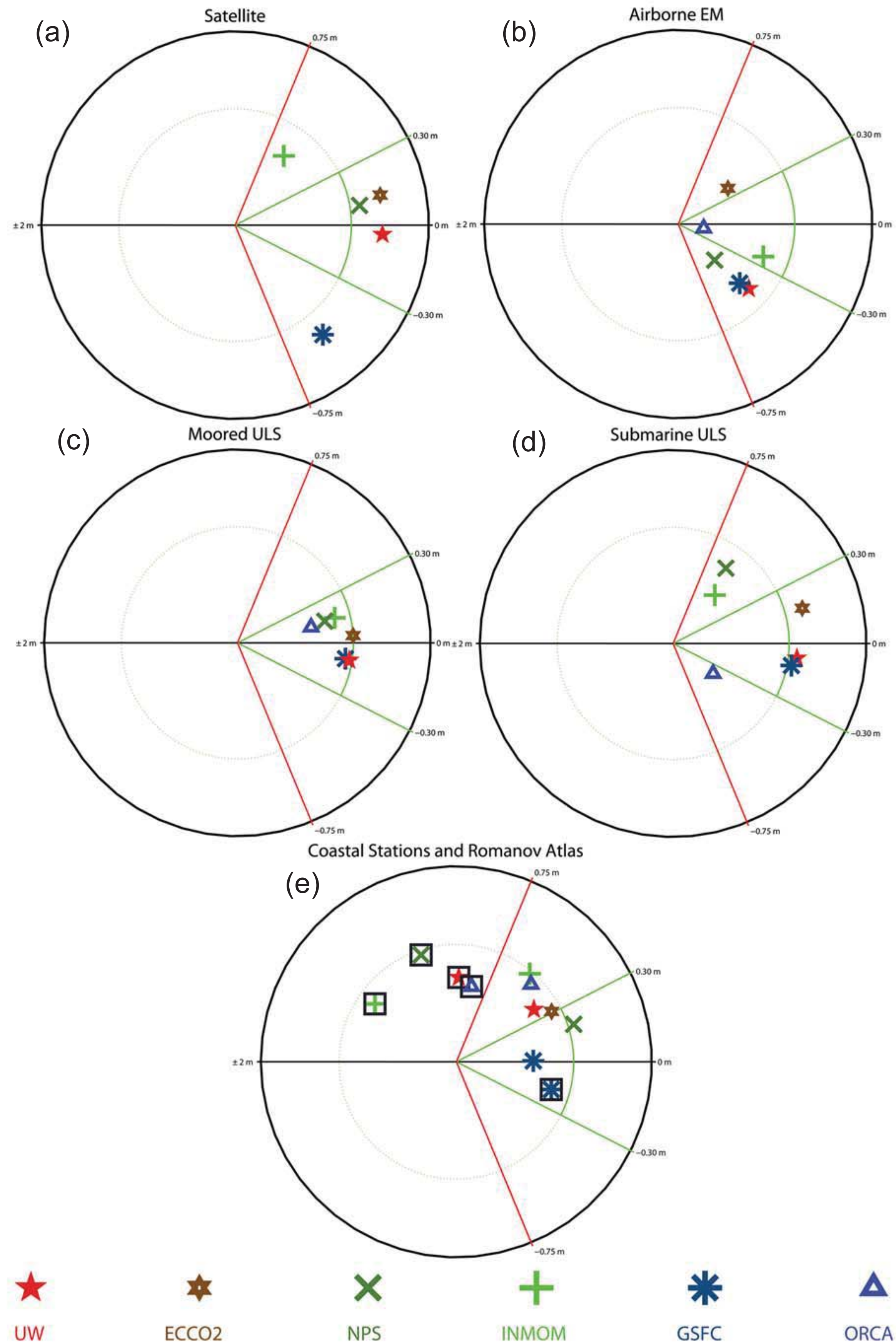

(a)
Satellite
(b)
Airborne EM
(c)
Moored ULS
(d)
Submarine ULS
Coastal Stations and Romanov Atlas
(e)
0.75 m
0.30 m
0 m
−0.30 m
−0.75 m
± 2 m
UW
ECCO2
NPS
INMOM
GSFC
ORCA

Figure 5

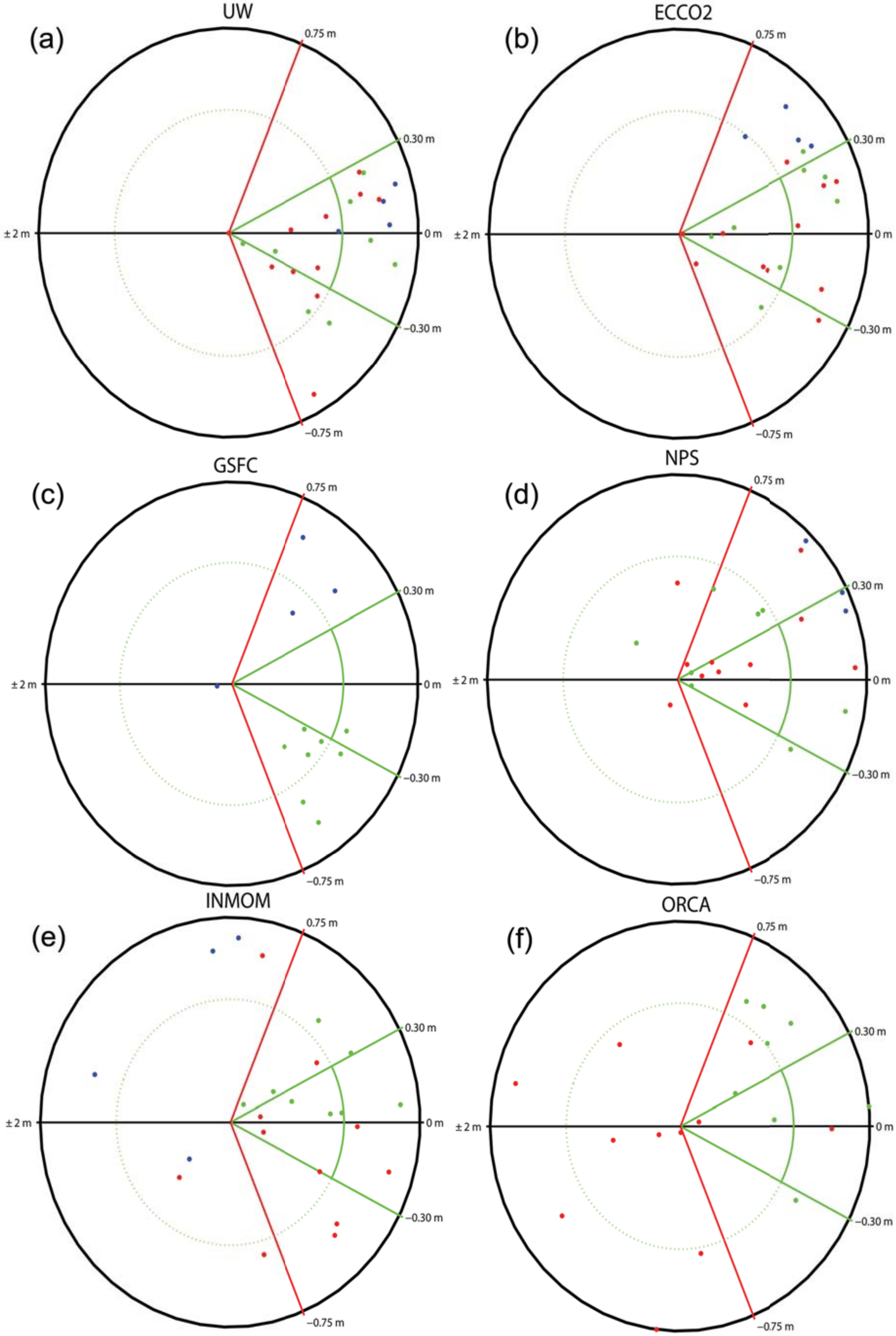

Figure 6

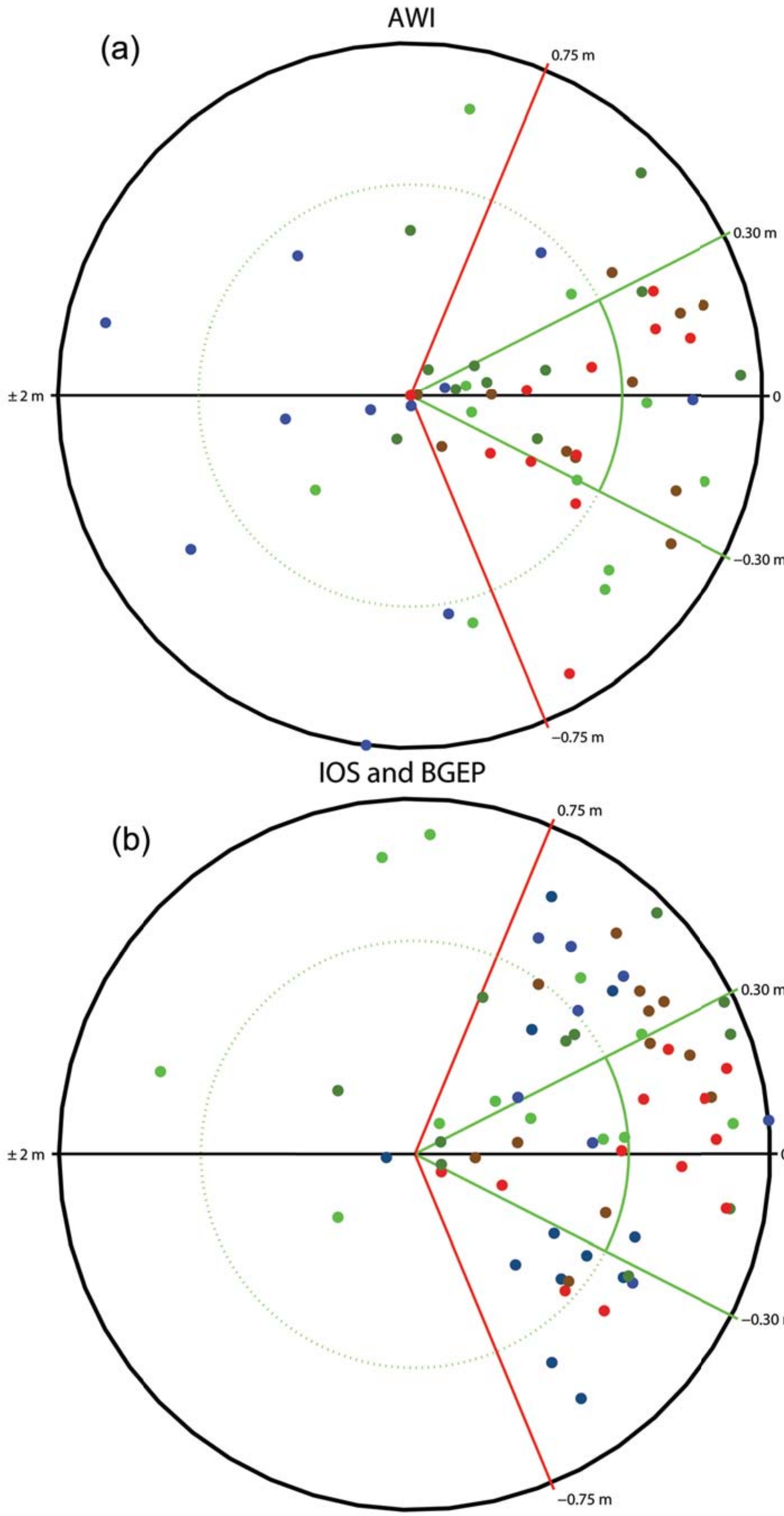
AWI
(a)
0.75 m
0.30 m
±2 m
0 m
−0.30 m
−0.75 m
IOS and BGEP
(b)
0.75 m
0.30 m
±2 m
0 m
−0.30 m
−0.75 m

Figure 7

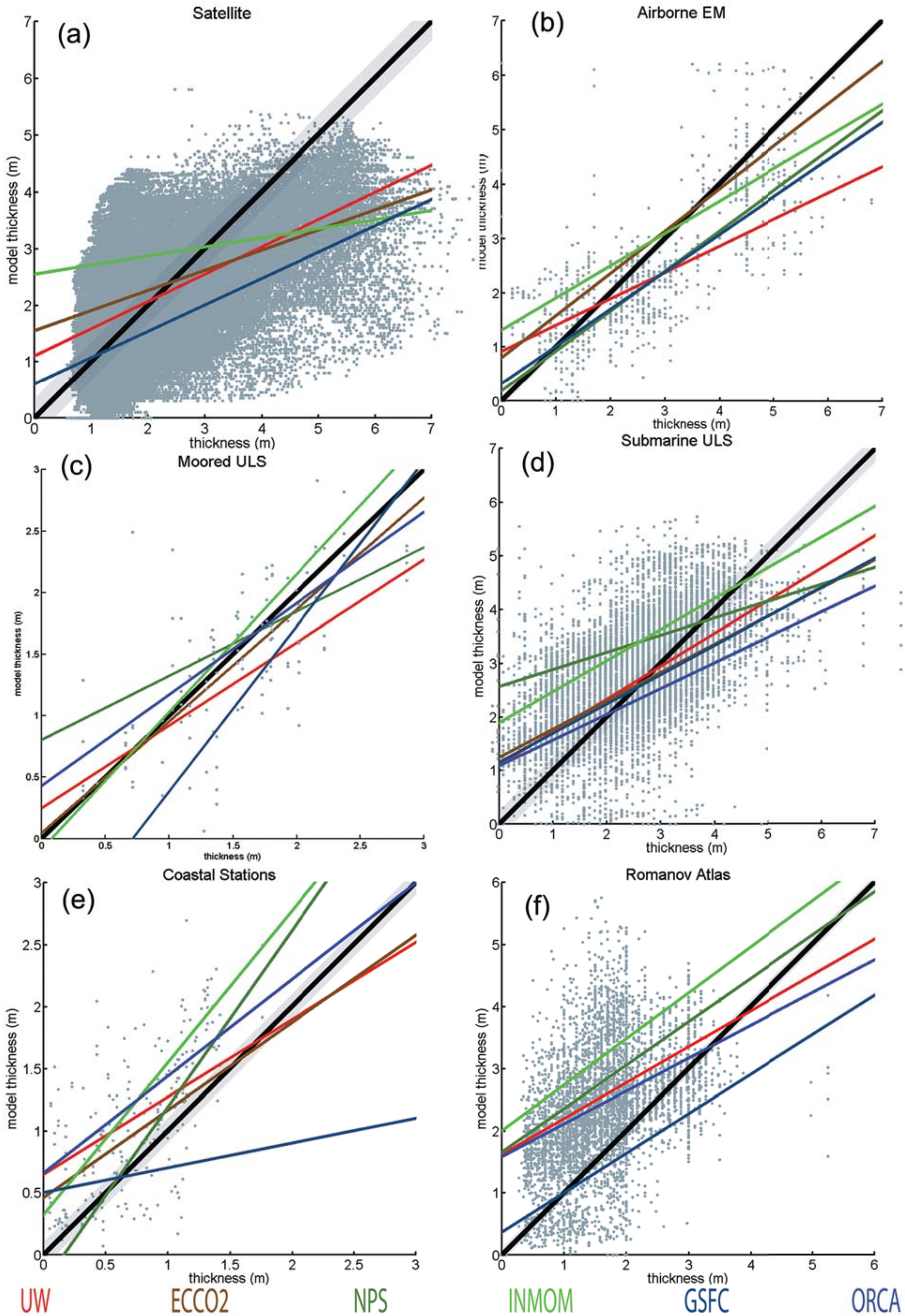
Satellite
(a)
model thickness (m)
thickness (m)
Airborne EM
(b)
thickness (m)
Moored ULS
(c)
model thickness (m)
thickness (m)
Submarine ULS
(d)
model thickness (m)
thickness (m)
Coastal Stations
(e)
model thickness (m)
thickness (m)
Romanov Atlas
(f)
model thickness (m)
thickness (m)
UW
ECCO2
NPS
INMOM
GSFC
ORCA

Figure 8